https://doi.org/10.5194/egusphere-2026-2371
Preprint. Discussion started: 18 June 2026


# Arctic-XBeach v1.0: A Python-Based Thermo-Morphodynamic Model for Arctic Permafrost Coastal Erosion

Kees Nederhoff[1], Kevin H. de Bruijn[2], Carola Seyfert[3], Li Erikson[4], Stuart G. Pearson[2], Robert McCall[3], Ferdinand K. J. Oberle[4], and Tom Ravens[5]

[1]Deltares USA: 8601 Georgia Ave 508, Silver Spring, MD 20910
[2]Delft University of Technology: Stevinweg 1, 2628 CN Delft, The Netherlands
[3]Deltares, Boussinesqweg 1, 2629 HV Delft, The Netherlands
[4]U.S. Geological Survey - Pacific Coastal and Marine Science Center, Santa Cruz, CA, USA
[5]University of Alaska Anchorage: 3211 Providence Drive, EIB 301P Anchorage, AK 99508

**Correspondence:** Kees Nederhoff (kees.nederhoff@deltares-usa.us) and Kevin H. de Bruijn (k.h.debruijn-1@tudelft.nl)

**Abstract.** Climate warming is leading to the erosion of Arctic permafrost coastlines at accelerating rates, with erosion up to 20 $\mathrm{m\,yr^{-1}}$ along the Alaska Beaufort Sea. Yet, accurate predictions of this erosion require coupling thermal permafrost dynamics with coastal hydro-morphodynamics, and current models are either computationally prohibitive for long-term simulations or omit important physical processes. To address these issues, a new open-source Python-based model called Arctic-XBeach was developed to couple the morphodynamic model XBeach to a one-dimensional enthalpy-based thermal module. A focus of this first version of Arctic-XBeach is on thermal denudation, the dominant erosion mechanism at sites where elevated beaches limit direct wave–bluff contact. Unlike prior implementations of thermal modules coupled with morphodynamic models, Arctic-XBeach uses an event-driven decoupling strategy. Specifically, the thermal module continues to calculate the evolution of the thawed layer during the year, but the morphodynamic module (XBeach) is only activated when simulated storms produce conditions under which thawed sediment is available for removal. Using this decoupled strategy results in a reduction of >99% in the number of calculations required for each time step in comparison to continuous coupling of the two modules. Validation of the model was performed at Barter Island, Alaska. Observed temperature trends were well-reproduced by the model (RMSE < 1.5 K), and the modeled trends in shoreline & bluff recession matched the observed trends (RMSE of 2.0–4.1 m over evaluation periods spanning 2–3 years each, compared to a total observed retreat of ∼112 m over 70 years with peaks of 6.6 $\mathrm{m\,yr^{-1}}$). Therefore, Arctic-XBeach has the potential to be used to run seasonal to decadal simulations of thermal-denudation dominated permafrost coastal changes, and also provides a flexible platform to integrate other Arctic-specific processes. Thermal abrasion and block-failure processes are planned as future extensions.

## 1 Introduction

Arctic shorelines, which comprise more than 30% of the global coastline, are particularly vulnerable to climate change because much of the coast consists of permafrost—perennially frozen ground—that becomes susceptible to erosion upon thawing (Lantuit et al., 2012). Arctic coastlines are either lithified (dominated by rock), or unlithified (dominated by sediments). Unlithified

https://doi.org/10.5194/egusphere-2026-2371
Preprint. Discussion started: 18 June 2026


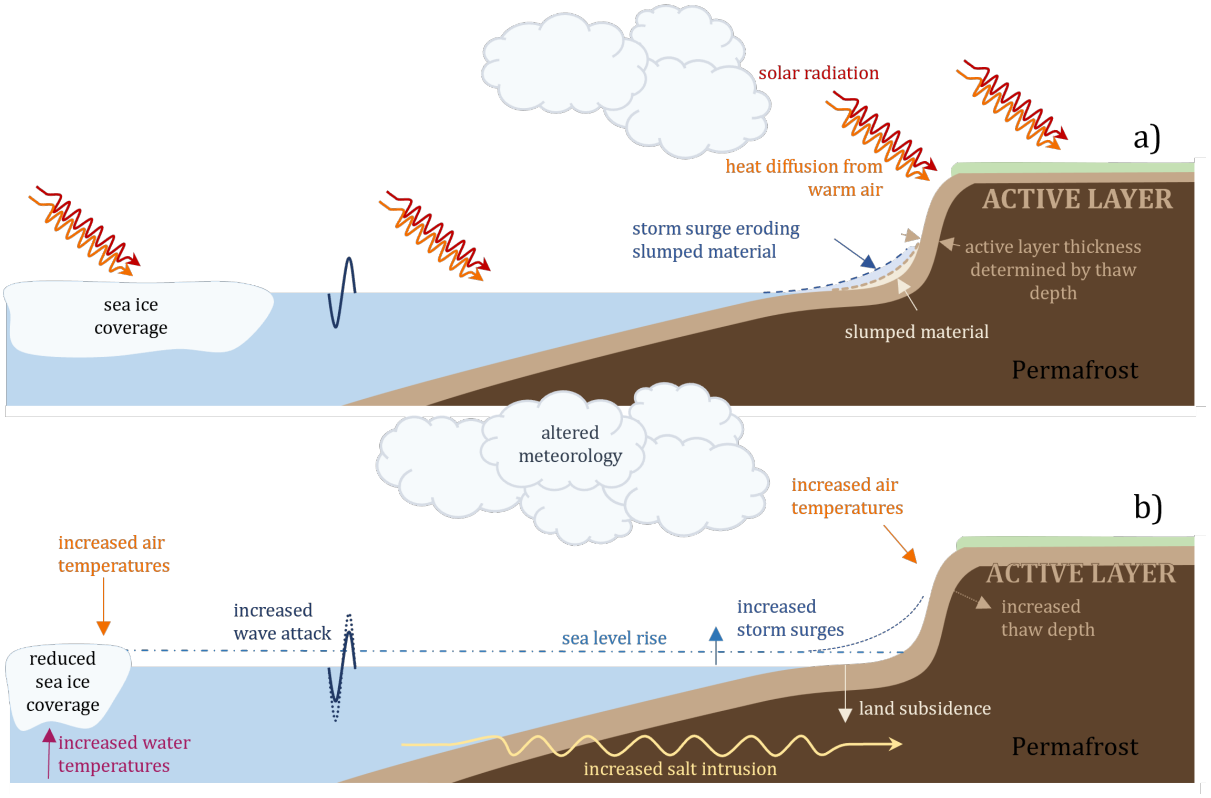


**Figure 1.** Schematization of coastal permafrost bluff erosion processes, specifically thermal denudation. a) Typical summer process conditions. b) Effects of the warming climate. If deeper layers start to thaw they become more susceptible to erosion. Thicker active layers lead to more slumping, and increases in frequency and magnitude of storm surges and wave energy lead to more transport of the protective slumped material and toe erosion.

.

permafrost coastlines are typically consolidated by ice and are susceptible to erosion when sediments thaw. The warming of the Arctic environment has led to accelerating coastal permafrost thaw, contributing to the increased observed erosion rates. The warming has also led to reduced sea ice and increased wave energy at the coast, which also contributes to the erosion (Overduin et al., 2014; Jones et al., 2020). Erosion rates in the historic time frame (1850-1940) were approximately 1 m/year but there has been an increase in erosion rates in recent years (Jones et al., 2009), with erosion rates on the Alaska Beaufort Sea reported as high as 20 m/year (Gibbs and Richmond, 2015). These trends are mirrored across the circum-Arctic, where permafrost coasts are retreating at accelerating rates (Irrgang et al., 2022). Erosion of these ice-rich coasts threatens infrastructure and ecosystems (Creel et al., 2024) and mobilizes large amounts of organic carbon that can amplify climate feedbacks (Terhaar et al., 2021). Permafrost bluff erosion is governed by the combined influence of thermal degradation and mechanical forcing. While thermal processes directly cause sloughing/erosion and precondition the bluff for failure, mechanical drivers, particularly wave attack, exert the dominant control on the rate and type of coastal retreat (Ravens and Peterson, 2021).

https://doi.org/10.5194/egusphere-2026-2371
Preprint. Discussion started: 18 June 2026


Two principal erosion mechanisms are responsible for much of the thermally driven permafrost bluff retreat in the Arctic: thermal abrasion and thermal denudation (Ravens and Peterson, 2021). Thermal abrasion, also referred to as niche erosion/block collapse, is predominant in coastal settings where no elevated beach separates the waves from the bluff face, allowing direct wave–bluff contact during storm surges. During storm surge events, the sea is in direct contact with the coastal bluff, and waves and currents thermally and mechanically cut a niche at its base (Kobayashi and Aktan, 1986). In the thermal abrasion mechanism, the permafrost thaw is largely driven by oceanic heat transfer. Typically, the depth of the niche will grow to about 5 or 10 m until the bluff collapses due to an overturning failure after the bluff is undermined (Hoque and Pollard, 2016). Following the collapse of the bluff, the fallen material provides a temporary protection to further bluff toe impacts, but will eventually be eroded (Ravens et al., 2012; Barnhart et al., 2014). Locations in Arctic Alaska where bluff retreat rates are approximately 5 to 25 m/yr are likely to experience thermal abrasion (Jones et al., 2009; Ravens and Peterson, 2021). Nairn et al. (1998) incorporated the thermal abrasion model of Kobayashi (1985) into their cross-shore sediment transport model (Nairn and Southgate, 1993), representing the effect of horizontal niche erosion as a vertically oriented scour hole. Although this approach was able to reproduce shoreline retreat behavior at various Arctic sites (Kobayashi et al., 1999; Pearson et al., 2016), it was hampered by its inability to correctly simulate block erosion.

Ravens et al. (2012) developed a process-based and predictive model of Arctic permafrost bluff retreat due to thermal abrasion and block erosion. The model considered 12- or 6-hour time segments and developed model-based calculations of nearshore water level, waves, and water temperature. When the water level at the coast was sufficiently high and when there were no fallen blocks before the bluff, the model simulated niche erosion using the Kobayashi (1985) model. Block collapse was assumed to occur when the cumulative niche depth reached a specified amount (e.g., 5 or 10 m depth). Barnhart et al. (2014) built on the work of Ravens by considering 1-hour time blocks and by computing the occurrence of block collapse based on geotechnical considerations. More recently, Bull et al. (2020) and Frederick et al. (2021) developed more sophisticated and computationally intensive thermo-mechanical models of the thermal abrasion mechanism, featuring 3D stress/strain fields and a plasticity model for permafrost. Most recently, Bayat et al. (2026) presented the Arctic Coastal Erosion Model, calibrated at Drew Point, Alaska.

Thermal denudation occurs when permafrost thaws as a result of thermal (atmospheric) heat transfer to the bluff face. Coastal bluffs experiencing thermal denudation are characterized by a high-elevation beach face that limits the amount of direct interaction between the beach face and the ocean. Thermal denudation can be broken into two processes: (1) thawing of the bluff face caused by short-wave radiation, long-wave radiation, latent heat fluxes, and sensible heat fluxes, and (2) the deposition of thawed bluff material onto the beach face, and subsequent offshore transport of beach material by wave action during high water levels. Many coastal bluffs in Arctic Alaska are experiencing thermal denudation where bluff retreat rates generally range from 0-3 m/year (Lantuit et al., 2012; Gibbs et al., 2021). Kasper et al. (2023) and Ravens et al. (2023) developed a process-based model of the thermal denudation mechanism and used this model to simulate bluff retreat at Foggy Island Bay, Alaska. These authors developed a 1D thermal model that estimated the daily thaw depth of the bluff face, and manually placed thawed material on the beach face. Storm-induced offshore sediment transport from the beach face was modeled using XBeach (Roelvink et al., 2009, 2018). Islam and Lubbad (2022) expanded upon previous research efforts

https://doi.org/10.5194/egusphere-2026-2371
Preprint. Discussion started: 18 June 2026


by simulating coastal bluff configurations that experienced both thermal abrasion and thermal denudation simultaneously. However, these authors did not include the contribution of solar (shortwave) radiation, long wave radiation, and latent heat flux in their XBeach morphodynamic model.

While significant progress has been made in developing Arctic coastal erosion models in the past couple of decades, there remains a need for an open-source model capable of simulating the key processes (i.e., heat transfer, geotechnical stability, hydrodynamics) and that is able provide reliable predictions of Arctic bluff retreat rates. To achieve this goal, we are presenting Arctic-XBeach, a new open source modeling system written in Python that will integrate the well-known morphodynamic model XBeach (Roelvink et al., 2009, 2018) with a one-dimensional heat transfer model for thawing of permafrost. Unlike previous studies that implemented hydrodynamic-morphodynamic and thermal models to be coupled at all times and thus ran continually (Ravens et al., 2023), our implementation of Arctic-XBeach decouples the thermal and morphodynamic models. This means that the thermal model will continue to simulate the thawing of permafrost at all times to determine the active layer depth and thickness, whereas the computationally intensive XBeach model will be run only during storm events. This approach will allow for simulations of seasonal to decennial time-scales and preserve the important interaction between the thermal and morphodynamic processes. Arctic-XBeach is designed to allow users to add additional processes (e.g., varying soil properties or salinity effects) into the thermal model by simply adding them to the thermal model programmed in Python and will not require modification to the fundamental structure of the model.

The initial version of Arctic XBeach focuses on the thermal denudation erosion process. We demonstrate the model's applicability on a case study based at Barter Island, Alaska, during the 2000-2020 time period. Barter Island is particularly well-suited because it combines multi-decadal shoreline/bluff-change records with independent soil-temperature observations and forcing datasets needed to evaluate both the thermal and morphodynamic components (i.e., Erikson et al. (2020a)). Finally, we present model performance, limitations, and potential future model extension directions toward Arctic coastal hazard analysis and system modeling.

## 2 Model Formulation

### 2.1 Conceptual Framework

The thermo-morphological model Arctic-XBeach integrates a hydrodynamic–morphodynamic module (XBeach; Section 2.2) with a new thermal module (Section 2.3). Both components are integrated by a Python-based wrapper (see figure 3). The thermal component simulates freeze-thaw processes and runs continuously throughout the entire simulation, while XBeach is only activated at times of potential morphodynamic activity (i.e., storm events and scheduled inter-storm updates to simulate slumping/avalanching; see Section 2.4). XBeach, implemented in Fortran, takes care of the computationally demanding hydrodynamic and morphodynamic tasks. The coupling logic of the thermal and XBeach models is provided by the Python wrapper. At each coupling interval, the wrapper (i) advances the thermal column to update thaw depth, (ii) maps thaw depth into an XBeach erodibility mask, (iii) executes XBeach when activation criteria are met, and (iv) updates the thermal geometry and boundary conditions using the revised profile. By running the XBeach executable only when it is needed, the wrapper improves

https://doi.org/10.5194/egusphere-2026-2371
Preprint. Discussion started: 18 June 2026


computational efficiency without sacrificing the representation of key coastal processes. Section 2.4 describes further details about how the two modules share data and are coupled through the wrapper.

### 2.2 Hydrodynamics, waves and sediment (XBeach)

The hydrodynamic-morphodynamic core of Arctic-XBeach is the open-source XBeach model (Roelvink et al., 2009, 2018). XBeach solves the nonlinear shallow water equations that couple with a short-wave action balance and sediment transport to determine morphologic change. The XBeach model can be run either in "surfbeat" (infragravity or long-wave resolving) or "non-hydrostatic" (fully wave resolving) mode. In this study, we used XBeach version 1.24.6041 ("Halloween" release, October 2024) in surfbeat mode, in which short-wave groups are handled statistically using wave action balance, but long waves (infragravity waves) are resolved explicitly within the shallow-water equations. The model updates the bed levels based on the sediment transport gradients.

We utilised the same hydrodynamics-sediment modules as the original XBeach model (e.g., tested formulations for avalanching and wave-induced sediment transport). By default, XBeach assumes all bed material to be available for transport if the critical shear stress for the initiation of motion is exceeded. Our addition is to tie this morphodynamic activity to the active layer depth of the thermal module via an erodibility mask (see Section 2.3). In practice, the mask identifies the non-erodible (frozen) areas and sets the sediment transport and/or bed update terms to zero in these locations while leaving the standard XBeach formulations intact where the mask indicates erodible (thawed) material. The result is that only the thawed areas of the bluff can be eroded and thus prevent erosion from occurring during early or late season storms while the bluff remains frozen. This method encapsulates the key physics of Arctic permafrost coastlines: thawed area controls sediment availability while the storm-driven hydrodynamics provide the dominant erosive forces. By replacing purely hydrodynamic erodibility thresholds with a thermally driven erodibility mask, Arctic-XBeach produces more realistic timing and magnitude of erosion on seasonal to decadal runs.

### 2.3 Thermal model

The thermal module of Arctic-XBeach simulates the evolution of the ground temperature profile and the active layer thickness, which is a direct constraint on the volume of erodible materials available for the morphodynamic model of XBeach. The main goal of the module is to calculate the thaw depth, which determines the erodibility mask of the coupled model (for more details, see Section 2.2). All soil thermal properties (conductivity, heat capacity, ice content) can be specified as depth-varying profiles to represent the transition from organic-rich surface layers to mineral substrates; the detailed parameterization is described in Section 3.5.2.

#### 2.3.1 Enthalpy and temperature

For the reasons outlined above, a standard heat-conduction approach without phase-change does not suffice when considering the importance of both temperature and phase change of the soil in the context of Arctic coastal erosion. Therefore, we employ

https://doi.org/10.5194/egusphere-2026-2371
Preprint. Discussion started: 18 June 2026


an enthalpy-based formulation of the transient heat conduction equation, including phase change (Hu and Argyropoulos, 1996; Ravens et al., 2023):

$$\rho \frac{\partial h}{\partial t} = \frac{\partial}{\partial z}\left(k \frac{\partial T}{\partial z}\right), \tag{1}$$

where $\rho$ is the bulk soil density $[\mathrm{kg\,m^{-3}}]$, $h$ is the specific enthalpy $[\mathrm{J\,kg^{-1}}]$, $k$ is the thermal conductivity $[\mathrm{W\,m^{-1}\,K^{-1}}]$, $T$ is the soil temperature $[\mathrm{K}]$, $t$ is time $[\mathrm{s}]$, and $z$ is the coordinate perpendicular to the soil surface (bluff face or sea floor) $[\mathrm{m}]$, positive in the landward direction.

In this conceptual framework, enthalpy is defined as the sum of the sensible thermal energy and latent heat due to phase changes of non-saline pore water. We assume that there is no influence from pore pressure, salinity, or ice-wedge heterogeneity. The influence of pore water salinity on freezing point depression is not included in this version; this limitation is discussed in Section 5. The complete temperature–enthalpy relationship contains three regimes representing the solid, liquid, and gas phases (Figure 2). For each phase, the temperature increases with enthalpy almost linearly. The energy added beyond the freezing temperature is used for the latent heat of fusion to melt pore ice at the solid–liquid transition near the melting point $T_m$. When all the pore ice has melted, further energy addition will increase the temperature in the liquid phase. The liquid–gas transition represented in the figure corresponds to the latent heat of vaporization and is only included for completeness and clarity, although temperatures in this study are well below the boiling point.

The enthalpy-based approach employed here naturally incorporates freeze–thaw dynamics and the lag in temperature response during phase transitions. The enthalpy-based approach resolves the freeze–thaw transition and provides a thaw-depth (active layer thickness).

Mathematically, this relationship can be expressed as

$$T = \begin{cases} \dfrac{h}{c_s}, & h < c_s T_m, \\ T_m, & c_s T_m \le h < c_s T_m + L n_b, \\ \dfrac{h - (c_s - c_l) T_m - L n_b}{c_l}, & h \ge c_s T_m + L n_b, \end{cases} \tag{2}$$

where $c_s$ and $c_l$ are the specific heat capacities of frozen and unfrozen soil, respectively $[\mathrm{J\,kg^{-1}\,K^{-1}}]$, $T_m$ is the melting (freezing) temperature of pore water $[\mathrm{K}]$, $L$ is the latent heat of fusion of water–ice $[\mathrm{J\,kg^{-1}}]$, and $n_b$ is the volumetric water/ice content $[-]$, defined as the volume fraction of pore space occupied by water or ice. Strictly, the latent heat contribution per unit mass of bulk soil requires a density correction factor $\rho_w/\rho$, i.e. $L \cdot (\rho_w/\rho) \cdot n_b$, to convert from energy per unit mass of water to energy per unit mass of bulk soil. In our implementation, this correction is omitted and absorbed into the calibrated $n_b$ values. Because $n_b$ is calibrated rather than independently measured, the effective $n_b$ compensates for the missing density

https://doi.org/10.5194/egusphere-2026-2371
Preprint. Discussion started: 18 June 2026


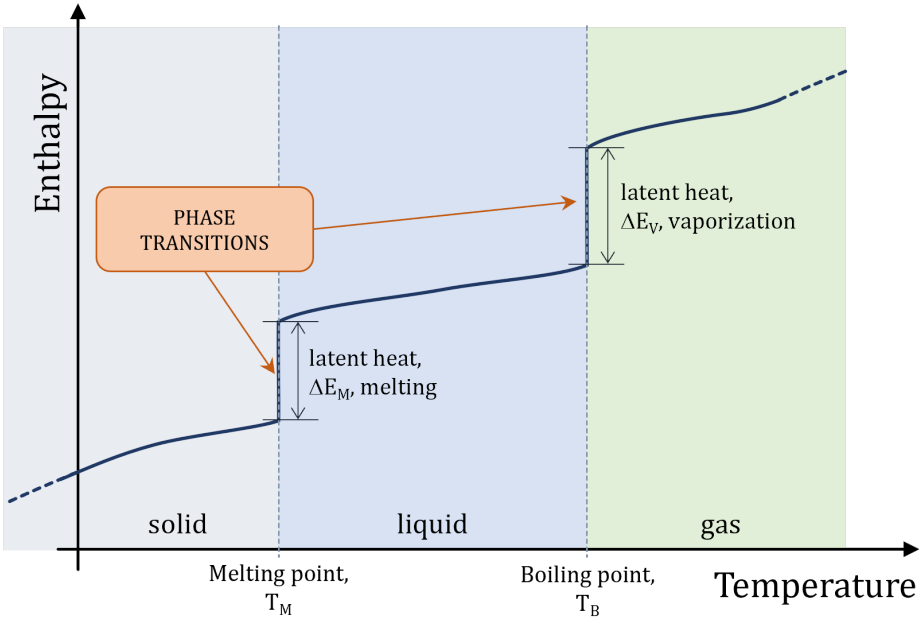


**Figure 2.** Conceptual enthalpy–temperature relation for freshwater. Temperature rises with enthalpy until the melting point, where added energy is absorbed as latent heat; after complete melting, temperature increases again. In reality, salinity and pressure can shift the phase-change interval, but those effects are not depicted here.

ratio, and the enthalpy formulation remains internally consistent. However, users should be aware that the calibrated $n_b$ values are consequently *effective* parameters that may differ from independently measured volumetric water contents by a factor of approximately $\rho/\rho_w$.

This enthalpy formulation (Equation 2) ensures that the model captures the thermal characteristics of permafrost soils. As shown in Figure 2, it accounts for the temperature plateau observed at the melting point during freeze-thaw transitions.

Throughout this manuscript, we will refer to *specific* heat capacity $c$ $[\mathrm{J\,kg^{-1}\,K^{-1}}]$, which is defined per unit mass, and *volumetric* heat capacity $C$ $[\mathrm{J\,m^{-3}\,K^{-1}}]$, which is defined per unit volume. These are related through the formula: $C = \rho c$. The enthalpy formulation (Equation 2) uses specific heat capacities ($c_s$, $c_l$) since enthalpy $h$ is defined per unit mass. The calibration parameters in Table 1 have been reported as volumetric heat capacities ($C_s$, $C_l$); this is common practice in soil thermal modeling.

https://doi.org/10.5194/egusphere-2026-2371
Preprint. Discussion started: 18 June 2026


### 2.3.2 Numerical solution and time-stepping

The enthalpy-based heat equation is discretized on 1D grids oriented perpendicular to the soil surface (bluff face above water, sea floor below) using a Forward-Time Central-Space (FTCS) finite difference scheme. This scheme is second order accurate in space and first order accurate in time. Soil thermal properties, such as thermal conductivity ($k$) and volumetric heat capacity ($C$), are updated at every step to account for frozen or thawed soil conditions.

The explicit FTCS discretization of Equation (1) for cell $m$ at thermal sub-step $n$ is written as:

$$h_m^{n+1} = h_m^n + \frac{k_m \, \Delta t}{\rho \, \Delta z^2} \left( T_{m-1}^n - 2T_m^n + T_{m+1}^n \right), \tag{3}$$

where $h_m^n$ is the enthalpy at cell $m$ and sub-step $n$, $k_m$ is the thermal conductivity at cell $m$ [$\mathrm{W\,m^{-1}\,K^{-1}}$], $\rho$ is the soil density [$\mathrm{kg\,m^{-3}}$], $\Delta z$ is the grid spacing along the surface-normal coordinate [$\mathrm{m}$], and $\Delta t$ is the thermal sub-time step [$\mathrm{s}$].

The Fourier number, or $F_o$, provides a way to assess the stability of the explicit FTCS discretization applied to the enthalpy equation. The Fourier number is calculated as follows: $\mathrm{Fo} = \alpha \Delta t / \Delta z^2$, where $\alpha$ is the thermal diffusivity, or the ratio of thermal conductivity ($k$) to volumetric heat capacity ($C$). The thermal diffusivity will vary based on the type of phase that the soil is currently in, so there is no one equation for assessing the stability of the enthalpy equation. However, stability can be evaluated by examining the limiting cases of the nonlinear system of equations, which include (i) a completely frozen soil, and (ii) a completely unfrozen soil. These limiting cases provide estimates for the maximum and minimum thermal diffusivity for any given case, and therefore provide estimates of the most and least stable conditions for the enthalpy equation. As long as the numerical scheme used to solve the enthalpy equation is stable when evaluating the limiting cases of completely frozen and completely unfrozen soils, it will be stable for all other intermediate cases where the soil is undergoing phase change. In both cases, the computed Fourier numbers were well below the standard explicit-scheme stability criterion of $\mathrm{Fo} \leq 0.5$ (Patankar, 1980) (approximately 0.14 and 0.02 respectively, for a thermal time step of 120 seconds and a layer thickness of approximately 0.05 meters with $N = 200$ nodes over a 10 m domain), providing sufficient margin for stable computations. Therefore, through numerical testing and the evaluation of these limiting cases, we selected a uniform thermal time step of 120 seconds (or 2 minutes) and $N = 200$ nodes over a 10 m domain ($\Delta z = L_z/(N-1) \approx 0.050$ m) to provide stable and convergent solutions.

### 2.3.3 Boundary conditions

Boundary conditions in the thermal module are defined at the top (soil surface) and bottom (deep ground) of the one-dimensional thermal column. We implement these boundary conditions using the ghost node method (Coco et al., 2014). Ghost nodes are virtual grid points placed outside the physical domain boundaries, used to enforce flux-type boundary conditions while maintaining second-order spatial accuracy. The method extends the computational domain beyond the physical boundaries to enforce flux-type (Neumann) conditions with second-order spatial accuracy (similar to the rest of the domain).

https://doi.org/10.5194/egusphere-2026-2371
Preprint. Discussion started: 18 June 2026


**Grid configuration.** The computational grid consists of $N$ interior nodes indexed $m = 0, 1, 2, \ldots, N-1$, where node $m = 0$ represents the physical surface and node $m = N-1$ represents the bottom boundary. Two additional ghost nodes — artificial grid points placed outside the physical domain solely to impose the prescribed boundary fluxes — are introduced: one above the surface (index $-1$) and one below the bottom (index $N$). The vertical grid spacing is uniform with $\Delta z = L_z/(N-1)$, where $L_z$ is the total domain depth (typically 10 m).

**Ghost-node formulation for Neumann conditions.** Consider prescribing a temperature gradient at a boundary node $m_b$ using a Neumann condition of the form $\partial T/\partial z|_{m_b} = G$, where the bluff-face perpendicular coordinate $z$ is positive in the landward direction. To enforce this condition with second-order accuracy, we use a three-point central difference centered at the boundary node to compute the temperature gradient as follows:

$$\left.\frac{\partial T}{\partial z}\right|_{m_b} \approx \frac{T_{m_b+1} - T_{m_b-1}}{2\Delta z} + O(\Delta z^2), \tag{4}$$

where $T_{m_b-1}$ is the ghost node on the *outside* of the domain and $T_{m_b+1}$ is the first interior node on the *inside*. Substituting (4) into Neumann equation and solving for the ghost-node temperature yields

$$T_{m_b-1} = T_{m_b+1} - 2\Delta z\, G. \tag{5}$$

This expression is the core of the ghost-node method. Once $G$ is specified from the physical boundary condition (for example, a geothermal gradient or surface heat flux), the corresponding ghost-node temperature can be calculated using (5). Note that the factor $2\Delta z$ appears in (5), rather than $\Delta z$. This is because the central difference spans two grid spacings between the ghost node $m_b - 1$ and the first interior node $m_b + 1$, which is necessary to achieve second-order accuracy.

**Lower boundary condition (geothermal gradient).** We prescribe a fixed geothermal gradient at the lower boundary ($m_b = N-1$), consistent with observations from the North Slope of Alaska (Lowell and Rona, 2005). We impose gradients of $g_{\mathrm{geo}} = 0.020 - 0.030$ K m$^{-1}$. We then use the ghost-node method to calculate the temperature at the bottom ghost node as follows:

$$T_N = T_{N-2} + 2\Delta z\, g_{\mathrm{geo}}. \tag{6}$$

This ensures that the FTCS stencil at node $m = N-1$ calculates a geothermal heat flux that is consistent with the prescribed gradient.

**Upper boundary condition (surface heat flux).** At the upper boundary ($m_b = 0$), we specify the boundary condition as a net surface heat flux $q_n$ [W m$^{-2}$]. We combine convective, radiative, and latent components as follows:

$$q_n = q_{\mathrm{convective}} + q_{\mathrm{radiation}} + q_{\mathrm{latent}}$$

https://doi.org/10.5194/egusphere-2026-2371
Preprint. Discussion started: 18 June 2026


Here, $q_n > 0$ denotes a net heat flux directed into the soil (i.e., in the positive $z$ direction). Using Fourier's law and the ghost-node relation, the surface ghost-node temperature is given directly by

$$T_{-1} = T_1 + \frac{2\Delta z}{k} q_n. \tag{7}$$

A positive $q_n$ increases the ghost-node temperature above $T_1$, creating a temperature gradient that drives heat into the domain through the FTCS stencil (Equation 3). This sign convention is consistent with Equation 9 below, where $q_{\text{convective}} > 0$ when the external medium is warmer than the soil.

In the following paragraphs, the individual components of the surface heat flux, convective, radiative, and latent, are described in detail.

**Convective heat flux** The convective heat transfer into the frozen soil is a function of the convective heat transfer coefficient, denoted as $h_c$, and the temperature difference between the soil and the surrounding medium at the interface. The determination of $h_c$ will depend on the external medium, which can be either water or air. Determination of $h_c$ for air is relatively simple and is given by (8) (Man, 2023).

$$h_{c,\text{air}} = \frac{0.0296 \left( v_w \frac{L_e}{\nu_{\text{air}}} \right)^{4/5} Pr^{1/3} k_{\text{air}}}{L_e}, \tag{8}$$

where $h_{c,\text{air}}$ is the convective heat transfer coefficient for the soil-air interface $[\mathrm{W\,m^{-2}\,K^{-1}}]$, $v_w$ is the wind speed at 10 m height from forcing data $[\mathrm{m\,s^{-1}}]$, $L_e$ is the convective length scale $[\mathrm{m}]$, here taken as 0.003 m, $\nu_{\text{air}}$ is the kinematic viscosity of air $[\mathrm{m^2\,s^{-1}}]$, with a typical value of $1.33 \times 10^{-5}$, $Pr$ is the Prandtl number $[-]$, typically 0.71 for air, and $k_{\text{air}}$ is the thermal conductivity of air $[\mathrm{W\,m^{-1}\,K^{-1}}]$, taken as 0.024.

Determining convective heat transfer through a soil-water interface subjected to waves, is less straightforward. Kobayashi et al. (1999) developed a formulation for breaking waves inducing thermal abrasion of a cliff, relating the heat transfer coefficient to near-bed orbital velocity. However, since there is limited validation data available in Arctic settings, we have employed a constant value of $h_{c,\text{water}} = 500\ \mathrm{W\,m^{-2}\,K^{-1}}$ as a pragmatic first approximation. This value is consistent with the order of magnitude for turbulent heat transfer in shallow, cold coastal waters (Kobayashi et al., 1999) and represents a practical first approximation in the absence of site-specific measurements. A natural extension would be to link $h_{c,\text{water}}$ to the near-bed orbital velocity $u_{\text{rms}}$ computed by XBeach, so that the heat transfer coefficient could be dynamically adjusted based upon local wave conditions. For submerged portions of the profile, we assume that surface fluxes associated with shortwave radiation, longwave radiation, and latent heat do not contribute to the thermal boundary condition; only convective heat transfer through the water column is considered.

We have now defined our convective heat transfer coefficients for both interfaces (soil/air and soil/water). Therefore we can calculate the convective heat flux through equation 9.

https://doi.org/10.5194/egusphere-2026-2371
Preprint. Discussion started: 18 June 2026


$$q_{\text{convective}} = h_{c,\text{air/water}} \left(T_{\text{air/water}} - T_{\text{soil}}\right) \tag{9}$$

We chose the above sign convention so that $q_{\text{convective}} > 0$ if the external medium is warmer than the soil, as positive flux is directed toward the soil.

**Radiation flux & solar flux calculator** The total net radiative flux includes the net influx of shortwave and longwave radiation. Due to the assumption of flat terrain in standard shortwave radiation data sets, we used a solar flux calculator to adjust for inclined surfaces (e.g., permafrost bluffs), according to (Kasper et al., 2023). Adjusting for inclination is especially important in the Arctic, where the low solar elevation angles, combined with the occurrence of polar day, result in prolonged and highly angle-dependent solar exposure of sloping bluff faces. The intensity of the sun on an inclined surface is given by:

$$I = I_0 \, p^{1/\sin A} \sin\theta, \tag{10}$$

where $I$ is the solar intensity [$\mathrm{W\,m^{-2}}$], $I_0$ is the solar constant [$\mathrm{W\,m^{-2}}$], $p$ is the atmospheric transmission coefficient [-] (dependent on altitude, weather conditions, and atmospheric composition), $A$ is the solar altitude angle [rad], and $\theta$ is the angle between the incoming solar radiation and the inclined surface plane [rad], accounting for surface slope (Buffo et al., 1972).

We can relate the flat-surface radiation to the inclined surface using:

$$I_{\text{inclined}} = I_{\text{flat}} \cdot \frac{\sin\theta_{\text{inclined}}}{\sin\theta_{\text{flat}}} = I_{\text{flat}} \cdot r, \tag{11}$$

where $r$ is the enhancement factor, which is computed dynamically based on the geometry (slope, aspect, latitude, time of year). Since the atmospheric transmission term $p^{1/\sin A}$ is common to both $I_{\text{inclined}}$ and $I_{\text{flat}}$, this term cancels out in the ratio, and $r$ depends only on geometric parameters.

As longwave radiation is emitted from the atmosphere as a whole, rather than directly from the sun, we assumed that the surface angle does not affect the net flux of heat related to longwave radiation. Similarly, we assumed that the surface latent heat flux was not affected by the surface angle.

### 2.4 Coupling with XBeach

This section discusses how the thermal module interacts with the XBeach model. The thermal module numerically updates the ground temperature at every thermal time step during the entire simulation, accounting for seasonal freeze-thaw cycles. After evaluating the forcing conditions, Arctic-XBeach determines whether to invoke the XBeach hydrodynamic-morphodynamic solver. During the coupling process, the active layer thickness, as calculated by the thermal module, is passed to XBeach as

https://doi.org/10.5194/egusphere-2026-2371
Preprint. Discussion started: 18 June 2026


an erodibility mask. Material in thawed cells is allowed to erode due to wave action or avalanching; however, frozen cells are considered non-erodible. Using this decoupled approach allows for increased computational efficiency, as the XBeach model does not need to be run during early-season storms with frozen bluffs causing little to no erosion (see Figure 3). In reality, Arctic-XBeach checks every time XBeach needs to be run at a given time interval. The coupling time step is 1 hr, while the time step for the thermal solver is 120 sec, providing approximately 30 thermal solutions during every coupling time step.

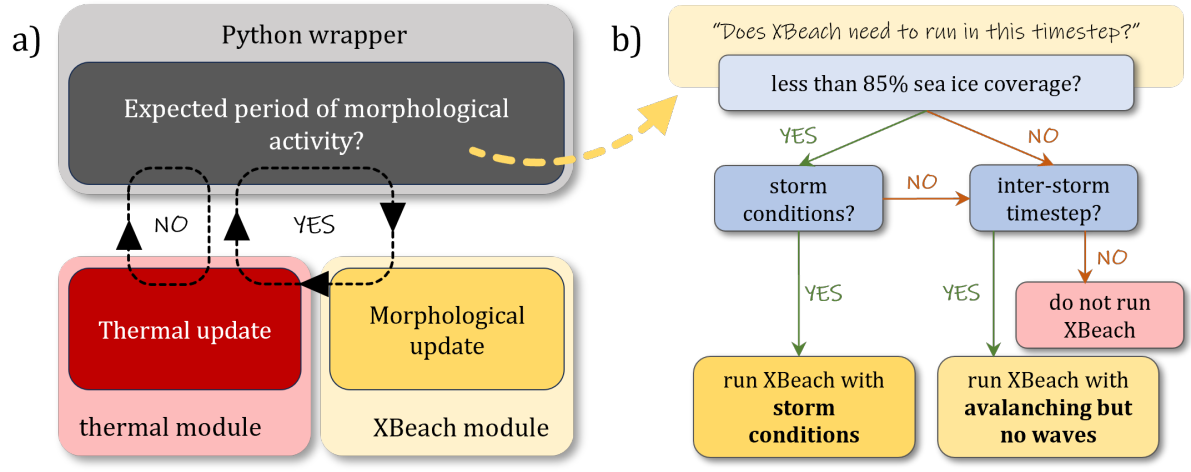


**Figure 3.** a) visualization of the conceptual framework of the python wrapper, including both the XBeach module and the thermal module. No matter whether a morphological update is supplied during a timestep, there will always be a thermal update. b) visualization of the decision tree within the Python wrapper for when to run the XBeach module, and when not to run it.

.

### 2.4.1 XBeach activation logic: when and why to run

Arctic-XBeach's coupling framework utilizes a collection of physical and practical criteria to determine whether to run XBeach or not. The decision tree implementing the XBeach activation logic is an effort to reduce computational cost while preserving accuracy in the erosion calculation. The Python wrapper module facilitates this activation via the following three criteria:

- **Sea ice presence** When sea ice cover exceeds a certain threshold (default = 85%) the forcing from waves is considered negligible, and therefore, XBeach is not activated. This is a reflection of the limitations of most global climate models (GCMs), which do not provide hydrodynamic information above this threshold.
- **Storm-driven activation:** Storm periods are determined by the comparison of the estimated wave run-up along the shore versus a user-specified threshold (typically the toe of the bluff). The empirical relationship of Stockdon et al. (2006) is used to estimate the run-up, which is then compared to the user-specified threshold. In cases where the estimated run-up is higher than the user-specified threshold, XBeach is activated to simulate potential changes in morphology. This choice was made to ensure that XBeach only runs when wave-driven processes have sufficient energy to remove slumped

https://doi.org/10.5194/egusphere-2026-2371
Preprint. Discussion started: 18 June 2026


material from the beach and increase erosion at the bluff toe. If $R_{2\%}$ (the highest 2% of run-up values) is lower than the toe, wave-driven erosion is unlikely to occur and the morphodynamic step may be skipped. The threshold value is usually selected to yield an average of 10 storm-driven activations per year. If the threshold value is lowered (frequent activations), simulated erosion is expected to increase and computational time is expected to increase. However, if the threshold value is raised (less frequent activations), simulated erosion is expected to decrease and computational time is expected to decrease.

- **Inter-storm interval:** To simulate bluff collapse not related to wave forcing, XBeach is run at a fixed interval regardless of whether storms are occurring. The interval between storms (default = 1 week) permits gravity-driven slumping of thaw-weakened bluff material using the XBeach morphological routines for avalanching. The intent is to (i) deliver slump debris to the toe between storms, (ii) update the topography and erodibility mask seen by the thermal module, and (iii) provide realistic initial conditions for subsequent storms.

Each of these conditions is evaluated at each coupling time step, but XBeach is only invoked when at least one of the conditions is true. The use of an event-driven scheme leads to a substantial reduction in the number of XBeach simulations. Depending upon the threshold selected, the activation threshold is expected to trigger 10 storm events per year. However, the total amount of time spent executing XBeach is typically a small fraction of a day per year (e.g., 3 days per year). Therefore, by invoking XBeach only during periods of high morphologic activity ( 1% of the year), the computational cost is reduced by > 99% compared to continuously running XBeach throughout the year.

### 2.4.2 Thaw Depth Calculation

The phase distribution in the ground determines the thickness of the thawed layer in XBeach and the thermal properties of the soil (thermal conductivity $k$ and heat capacity $C$). These thermal soil conditions depend on the phase of the soil and are adjusted dynamically by the thermal module using the enthalpy-temperature relationship (Equation 2).

To obtain the thaw depth that will be utilized as the erodibility mask for XBeach, we project the thaw interface from the thermal model's surface normal orientation to the vertical orientation of XBeach. The thermal model calculates the thaw depth along the surface normal direction at each surface node, using the first depth at which $T < T_m$ to define the thaw depth. These thaw depths are then approximated by connecting the points into a piecewise linear thaw interface roughly parallel to the ground surface. A vertical thaw thickness at each XBeach grid node is calculated by projecting this thaw interface onto the vertical coordinate of XBeach, defining the erodibility mask. This projection is required due to the thermal grid being aligned with respect to the potentially sloped bluff face and XBeach operating within a vertical coordinate system.

In early winter, there may be a thin layer of ice on top of soil that has already thawed, so that otherwise erodible materials are hidden underneath. Therefore, we use a freeze-thaw threshold, where the amount of frozen material is determined to identify if there is a sufficient amount of frozen material to hide the previously thawed material underneath. If the amount of frozen material above the ground surface is less than the threshold value (the default is 3 grid cells, or approximately 0.3 m), then the erodibility mask will continue to indicate that the previously thawed material beneath is susceptible to erosion. We support

https://doi.org/10.5194/egusphere-2026-2371
Preprint. Discussion started: 18 June 2026


this threshold value with surveys conducted at Barter Island and Barrow (Swarzenski et al., 2016; Schaefer et al., 2015). The application of this threshold value provides for a more physically accurate representation of how sediment is eroded during freeze-thaw cycles. However, we acknowledge that during very energetic storms, waves may break-up and move sediment even when those sediments have been partially frozen (Reimnitz and Maurer, 1979); this process is currently not incorporated into Arctic-XBeach.

#### 2.4.3 Data Exchange and Model Run

The interaction of the data exchange between the thermal model and the XBeach model is shown below;

1. The thaw depth is calculated and transferred from the thermal model to XBeach.
2. XBeach is run with the thaw depth used to update the erodibility mask (i.e., frozen cells are non-erodible).
3. Finally, XBeach delivers morphological change and recent water levels and these are fed back to the thermal module.

The above described coupling method allows for the exchange of information between the thermal and hydrodynamic models. It also provides two-way communication between the different models so as to allow for improved computational efficiency. A spin-up period of 10 years prior to the start of the study time frame was added to provide the initial subsurface conditions required to realistically simulate the subsurface conditions. This additional runtime allowed the thermal model to establish a stable vertical temperature distribution and ensured that deeper soil layers reached near-periodic seasonal cycles. While the equilibrium state in the upper and intermediate layers usually occurred in less than 5 years, the use of a full 10 year simulation provided the confidence level needed to ensure adequate representation of the thermal memory in the subsurface prior to simulating storm events.

## 3 Application to Barter Island, Alaska

We apply Arctic-XBeach to a segment of the northern permafrost bluff coastline of Barter Island to demonstrate and validate the model. The site is well-documented with rich observational datasets over multiple decades: historical imagery documents a multi-decadal average retreat rate of about 1.6 m $yr^{-1}$ (70-year mean), with episodic peaks reaching 6.6 m $yr^{-1}$ during 2012–2013 (Gibbs et al., 2021). Due to the availability of thermal observations along with bathymetric surveys and shoreline position data, Barter Island forms an ideal testbed for testing the capability of the model to reproduce the observed thermal and morphodynamic behavior under varying Arctic forcing conditions.

### 3.1 Site description

Barter Island is situated off the northern coast of Alaska, within the North Slope Borough, near 70.1 ° N and 143.7 ° W (panel A, Figure 4). The island hosts the Native community of Kaktovik, population 124 (United States Census Bureau, 2026) and an active Long Range Radar Site (LRRS) operated and owned by the U.S. Air Force. The north side of the island is primarily

https://doi.org/10.5194/egusphere-2026-2371
Preprint. Discussion started: 18 June 2026


composed of unlithified materials (Gibbs et al., 2021), similar to other areas along the Arctic Coastal Zone (Lantuit et al., 2012) in Alaska and Russia.

The site is a bimodal representation of sediment distribution, common to permafrost coastlines. Sediment on the beach is coarse sand with a mean diameter of 1.9 mm (Lantuit et al., 2012; Erikson et al., 2020a), whereas the sediment found on the bluff crests is much finer and can have a mean diameter of 0.03 mm or coarse silt (Oberle et al., 2026). We assume that the bluff sediments behave similarly to the beach sediments when they thaw and are therefore represented using an equivalent grain size parameterization, consistent with XBeach's non-cohesive sediment transport framework. This represents an important limitation of our modeling approach, which we discuss further in Section 5. The beach berm crest elevation exceeds the bluff toe elevation, so that under most storm conditions waves do not directly contact the bluff face. This configuration favors thermal denudation over thermal abrasion. Thermal denudation (slump and thaw of bluff faces) appears to be the primary means of coastal erosion at this site; however, it is possible that, in recent years, thermal abrasion events may also occur periodically during extreme storm surges (Ravens and Peterson, 2021).

The coast is exposed to waves between the break-up of sea ice in late June/early July and the formation of new sea ice in October (Nederhoff et al., 2022). During the open water season, the coast is exposed to storms from the northwest to northeast sectors. Gibbs et al. (2021) showed that the inter-annual variation in erosion rates at this site is highly correlated with the magnitude of various environmental factors, including the amount of energy input into the system via wave action, the number of positive degree days, the air and sea surface temperatures and the length of time that the sea ice remains absent from the coastline.

### 3.2 Input data

Initial conditions, boundary conditions, and forcing data are required to run the Arctic-XBeach model. Initial conditions define the bathymetric profile and initial ground temperature distribution. The initial conditions describe both the bathymetry (profile) of the sea floor and the initial temperature distribution in the ground. The boundary conditions refer to the wave action that comes from offshore and the thermal boundary conditions at the surface and in the ground. In particular, the forcing data are time-dependent boundary conditions and include time series representing the factors that drive the thermal and hydrodynamic processes within the model. In the next subsections, these components will be discussed in more detail.

#### 3.2.1 Bathymetric transect

Bathymetric data were used from Erikson et al. (2020b). They conducted surveys in 2010-2011 and collected a significant number of depth soundings and elevation data along 29 transects in which they surveyed the beach elevations. Due to the variability between transects in the availability of bathymetric data, which occurred both horizontally and vertically across the survey region, with minimal bathymetric data available in the offshore regions, a schematized bathymetric profile was developed for the model runs. The schematized bathymetric profile was created using a single representative transect that was selected based on expert opinion and the quality of the available data, as well as the typicalness of site conditions. The schematized bathymetric profile is composed of six sections: (1) a flat tundra section landward of the bluff, (2) a steep permafrost bluff face, (3) a narrow

https://doi.org/10.5194/egusphere-2026-2371
Preprint. Discussion started: 18 June 2026


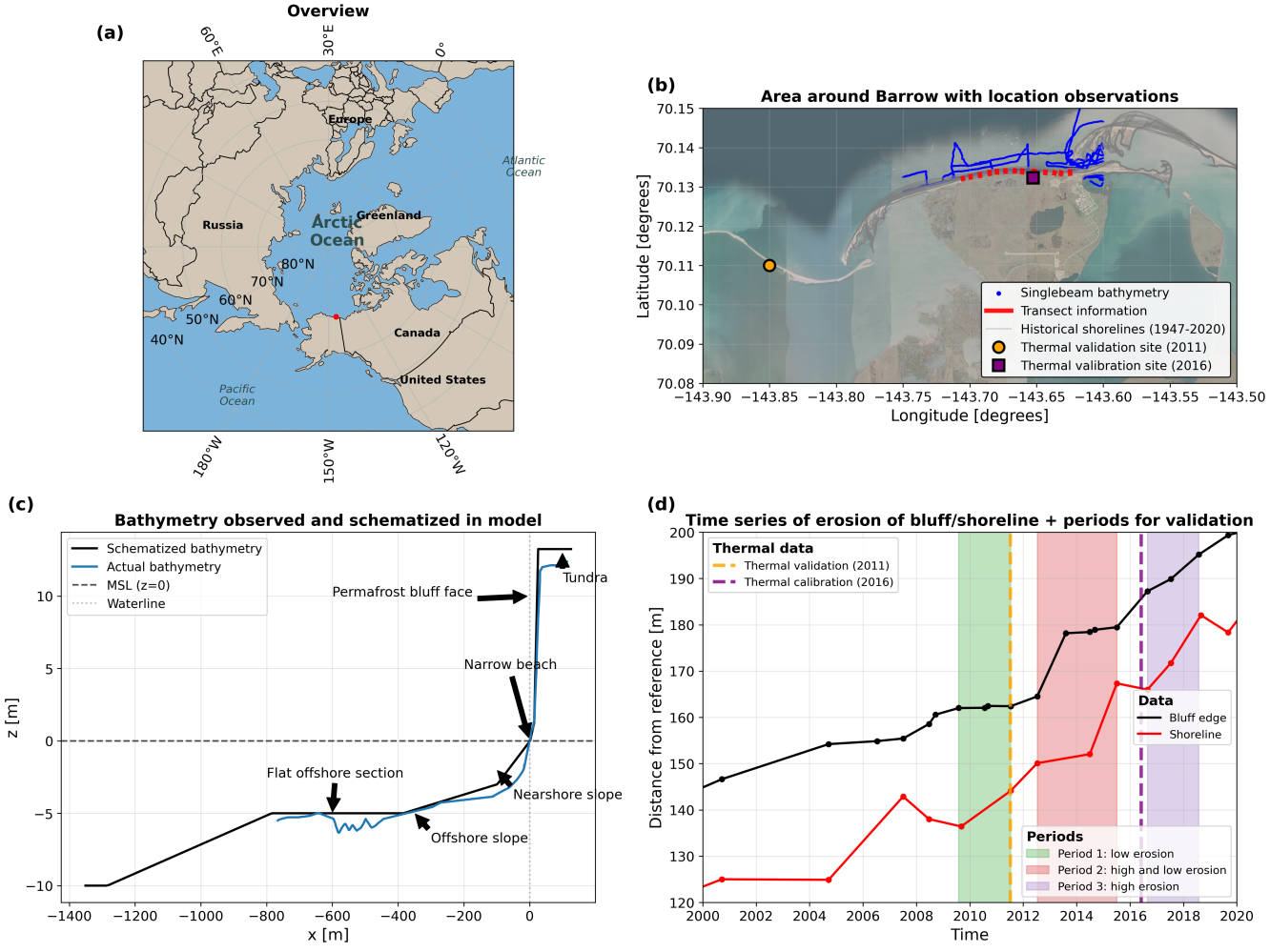


**Figure 4.** Study region overview, data sources, and conceptual model configuration. (a) Regional context for the study area of Barter Island, Alaska (red marker). (b) Satellite image of the study area at high resolution with all observation-based data used for model initialization and validation: single-beam bathymetric transects (blue), transect data (blue lines), historical shorelines between 1947 and 2020 (red), and thermal validation data (yellow) and calibration data (purple) (2011 and 2016 respectively). (c) Simplified cross-shore bathymetric profile from field observations (blue) and an idealized version of it used in the Arctic X-Beach model (black). Key geologic units identified include: offshore artificial slope, flat nearshore section, nearshore slope, beach, coastal bluff. (d) Observed time series of shoreline position (black) and bluff edge position (red) relative to a fixed reference line for the years 2000 through 2020 (Gibbs et al., 2021) The shaded regions indicate the three different erosion regimes used to validate the model performance: Period 1 (low erosion), Period 2 (both high and low erosion), Period 3 (high erosion). Vertical dashed lines represent the years that were used for thermal validation (2011) and thermal calibration (2016).

https://doi.org/10.5194/egusphere-2026-2371
Preprint. Discussion started: 18 June 2026


beach, (4) a nearshore slope extending to approximately 2 m depth, (5) an offshore slope transitioning to deeper water, and (6) a flat offshore section to accommodate the implementation of the equilibrium boundary condition in XBeach (Figure 4 panel C). The offshore flat section ensures stable application of XBeach's offshore boundary condition and avoids spurious reflection or profile adjustment at the boundary. The profile geometry parameters were constrained by the measured transect and adjusted within the observed ranges during sensitivity analyses.

#### 3.2.2 Initial ground temperature distribution

Initial soil temperature profiles were obtained from ERA5 reanalysis data (Hersbach et al., 2020) that provides soil temperature in four layers (0 to 7, 7 to 28, 28 to 100, and 100 to 289 cm depth) on a 0.25 °grid. The layer center temperatures were taken as the nodal values, which were linearly interpolated to produce a continuous initial profile for the vertical grid of the thermal model.

The ERA5 soil temperature data have significant systematic errors relative to the in situ measurements at Barter Island. We therefore used a spin-up phase to reduce sensitivities to uncertainty in the initial conditions. The spin-up length was determined by comparing annual cycles from successive one-year simulations. Year-to-year differences in the modeled temperature fields fell to less than 1 ∘K after approximately 3-5 years of spin up (depending upon depth). Ten years of spin up were used prior to the analysis period for the calibration and validation periods.

#### 3.2.3 Forcing data

Atmospheric and oceanic forcing inputs were based on a variety of source inputs. Energy fluxes at the surface (shortwave and longwave radiation; sensible and latent heat) were determined as hourly values from the closest land point of the ERA-5 atmospheric dataset that provided hourly values of air temperature, humidity, wind speed, cloud cover and sea ice fraction. These are the fluxes which provide the upper thermal boundary condition of the soil heat equation. Wave boundary conditions were specified by significant wave height ($H_s$) and peak wave period ($T_p$) from ERA5 ocean wave re-analysis (Hersbach et al., 2020) (converted from $T_{m01}$ using Goda (2010)). The waves were transformed from the nearest ocean ERA5 grid point to the model's offshore boundary as described in Engelstad et al. (2024). Water levels were specified by water levels as reported in Nederhoff (2025). We fully disabled storm-driven XBeach activation above an 85% ice concentration where open-water wave forcing is essentially absent or unreliable. Geothermal heat flux at the lower boundary was set to 0.0212 K $m^{-1}$.

### 3.3 Calibration and validation data

#### 3.3.1 Thermal observations

Soil temperature calibration and validation relied on two independent observational datasets. The first set of data were the measurements at 17 different soil depths that were collected during an approximate time period of 3.5 months (May 31, 2016 – Sept 14, 2016) that were used for model calibration (Foley et al., 2026). The second set of data provided by Erikson et al. (2020a) included soil temperature at four different soil layers spanning nearly three months (July 8–Sept 27, 2011) and were

https://doi.org/10.5194/egusphere-2026-2371
Preprint. Discussion started: 18 June 2026


used for independent validation. Therefore, this discrepancy was removed from our analysis. Both observation sites are located very near the shoreline of Barter Island (see Figure 4, Panel B)

#### 3.3.2 Shoreline position

Historical shoreline and bluff edge positions were obtained from Gibbs et al. (2021), who digitized coastal positions from aerial imagery spanning 1947-2020. We extracted bluff edge and shoreline positions relative to a fixed offshore baseline (Figure 4 panel D).

We chose the three following time periods for model evaluation with high erosion rate variability:

- **Period 1**; 2 August 2009 through 15 July 2011; Low Erosion Period (average retreat of 0.2 m/yr) - lower-than-average wave power, lower than average summer temperatures.
- **Period 2**; 11 July 2012 through 5 July 2015; Variable Erosion Period (average retreat of 5.0 m/yr); Moderate Wave Power and warmer summer temperatures.
- **Period 3**; 27 August 2016 through 30 July 2018; High Erosion Period (average retreat of 4.1 m/yr) - longer than normal ice-free season, higher-than-normal temperatures, sustained wave forcing.

Period 2 was used for coupled model calibration. Periods 1 and 3 were reserved for independent validation. The location of the shoreline and bluff edge is determined by a simple intersection with elevation +0 and +13 m+MSL.

### 3.4 Model setup

The model domain extends 100 m landward of the initial bluff crest to almost 1400 m offshore. This extent ensures that the offshore boundary is beyond the zone of significant morphological change, and also allows space for bluff retreat at the landward boundary over multi-year simulations. Variable resolution is used in the computational grid from XBeach to balance accuracy and efficiency. Finer resolution ($\Delta$x = 0.5 m) is applied in the nearshore and beach zone where morphological gradients are steepest and thermal-morphological coupling is most active. The grid spacing increases gradually offshore and onshore to $\Delta$x = 2 m in regions of gentler slopes. The vertical thermal grid extends to 10 m depth with $N = 200$ nodes, yielding a uniform spacing of $\Delta z = L_z/(N-1) \approx 0.050$ m.

XBeach uses an explicit numerical scheme and computes its own time step which was typically in the order of 0.2 s. The thermal model uses a constant time step of 2 minutes (120 seconds). In turn, the thermal model is updated with a revised bathymetry on an hourly basis, which also corresponds to the resolution of the input atmospheric forcing data. This multi-rate time stepping balances computational efficiency with accurate resolution of the different process timescales: wave periods, morphological adjustment and thermal evolution.

Key model parameters are set as follows. XBeach sediment transport parameters have been set largely to their default values, validated for sandy coasts (Roelvink et al., 2009), with only adjustments for parameters where there is field data to inform them (e.g. grain size to 36 $\mu$m) and minor calibration to other parameters. The morphological acceleration factor (morfac) is set to 1

https://doi.org/10.5194/egusphere-2026-2371
Preprint. Discussion started: 18 June 2026


(i.e., no acceleration) to preserve the correct temporal sequencing of thermal and morphological processes. Note that XBeach is developed for non-cohesive environments despite the relatively low grain size used.

## 3.5 Calibration

We use a two-step calibration strategy. First, we calibrate the standalone thermal model to reproduce observed temperature profiles, in order to reproduce realistic thaw depths prior to coupling with XBeach. Second, we calibrate the coupled Arctic-XBeach model with observed bluff retreat rates. Direct calibration of XBeach alone at Barter Island is not possible since erosion there is tightly controlled by thermal forcing; hydrodynamic forcing only cannot simulate observed morphodynamics without the correct thaw depth input. Since XBeach is a widely applied coastal model with validated default parameters (e.g. Roelvink et al. (2009)), we largely depend on default parameters for the hydro–morphodynamic module, but minor calibration to wave asymmetry and skewness related sediment transport parameters was performed, which controls the amount of onshore transport (see Section 3.5.2).

### 3.5.1 Thermal Model

The thermal module of Arctic-XBeach was calibrated using a minimum parameter physically constrained approach. Except for three thermodynamic property inputs, all other property inputs were determined as the literature values for known physical constants or solid materials. These included the latent heat of fusion ( $L$ ) , phase density ( $\rho_{\text{water}}$ , $\rho_{\text{ice}}$ , $\rho_{\text{particle}}$ ), and the melting temperature ( $T_m$ ). In addition, all model domain input parameters (maximum depth = 10m, and $N = 200$ vertical nodes yielding $\Delta z \approx 0.050$ m) were selected on the basis of the need to characterize the seasonal thermal dynamic processes at a morphological detail level which was deemed suitable for modeling purposes.

Optimization of calibration site specific parameters was restricted to those that are expected to vary substantially among Arctic coastal sites and cannot be estimated using available data alone. An automated hyperparameter optimization algorithm called Optuna (Akiba et al., 2019), was utilized to determine the optimal values for the site specific parameters that provided the best fit to the observed bore hole soil temperatures (See Section 3.3), during the 2016 calibration year, based on the root mean square error (RMSE) metric. The three site specific parameters that were optimized in this process were:

1. **Volumetric ice content** ($n_{b,\text{max}}$, $n_{b,\text{min}}$): Controls latent heat storage and has a very wide range of values (less than 0.3 in coarse sand and greater than 0.8 in ice-rich silt) that depend greatly upon soil type. These two parameters will control the thickness of the thawed layer of soil most strongly.

2. **Thermal conductivities** ($k_{\text{frozen}}$, $k_{\text{unfrozen}}$): Values can differ by 1 – 2 orders of magnitude depending on soil composition (e.g., mineralogy, organic content, porosity). In addition, we developed a function to describe depth-dependent profiles to characterize the normal transition from organic-rich surficial layers to mineral-based substrates (Farouki, 1981).

3. **Geothermal gradient** ($g_{\text{geo}}$: A site-specific geothermal gradient constrained to the 0.020 – 0.030 K m$^{-1}$ range, which is representative of the entire North Slope of Alaska (Lowell and Rona, 2005).

https://doi.org/10.5194/egusphere-2026-2371
Preprint. Discussion started: 18 June 2026


Calibration of volumetric heat capacity ($C_{\text{frozen}}$, $C_{\text{unfrozen}}$), which is physically bounded by reasonable values for soils and moisture content in permafrost systems, allowed for some minor variability as part of modeling the combined effect of soil and water content in permafrost environments where these factors cannot be easily measured. All calibration range boundaries (Table 1), based upon a large number of literature compilation sources for Arctic soils (Farouki, 1981), have been used as a basis for this calibration.The optimization was run for 1000 trials, producing a lowest RMSE of 1.06 K for the 2016 calibration period. Convergence analysis showed that the objective function stabilized after approximately 500 trials, with negligible improvement thereafter. A constrained calibration strategy was utilized so that all of the optimized model parameters remained physically meaningful and would be applicable to other Arctic coastal sites having a similar geology, instead of allowing the model parameters to become overly dependent upon site-specific measurements through excessive variability.

**Table 1.** Thermal module parameters: fixed values based on literature and calibrated site-specific properties. Only parameters marked as "Calibrated" were varied during optimization; all others were held constant. Final calibrated values achieved RMSE = 1.06 K.

| Parameter | Value/Range | Status | Source/Rationale |
|---|---|---|---|
| *Fixed parameters (literature values)* | | | |
| $T_m$ [K] | 273.15 | Fixed | Freshwater melting point at 0 °C |
| $L$ [J kg$^{-1}$] | 334,000 | Fixed | Latent heat of fusion |
| $\rho_{\text{water}}$ [kg m$^{-3}$] | 1000 | Fixed | Density of fresh water at $T_m$ |
| $\rho_{\text{ice}}$ [kg m$^{-3}$] | 917 | Fixed | Density of ice at $T_m$ |
| $\rho_{\text{particle}}$ [kg m$^{-3}$] | 2650 | Fixed | Quartz mineral density |
| $h_{c,\text{water}}$ [W m$^{-2}$ K$^{-1}$] | 500 | Fixed | Kobayashi et al. (1999) |
| max_depth [m] | 10 | Fixed | Exceeds seasonal damping |
| $\Delta z$ [m] | ≈0.050 | Fixed | $N = 200$ nodes over 10 m |
| *Calibrated parameters (site-specific)* | | | |
| $n_{b,\text{max}}$ | 0.25–0.90 | Calibrated: 0.710 | Ice-rich surface layer |
| $n_{b,\text{min}}$ | 0.25–0.78 | Calibrated: 0.470 | Deep soil ice content |
| $n_{b,\text{max depth}}$ [m] | 0.20–2.0 | Calibrated: 0.419 | Transition start depth |
| $n_{b,\text{min depth}}$ [m] | 0.50–5.0 | Calibrated: 2.372 | Transition end depth |
| $k_{\text{frozen,min}}$ [W m$^{-1}$ K$^{-1}$] | 0.70–3.24 | Calibrated: 0.905 | Surface frozen conductivity |
| $k_{\text{frozen,max}}$ [W m$^{-1}$ K$^{-1}$] | 0.70–3.70 | Calibrated: 1.731 | Deep frozen conductivity |
| $k_{\text{unfrozen,min}}$ [W m$^{-1}$ K$^{-1}$] | 0.30–1.60 | Calibrated: 0.330 | Surface thawed conductivity |
| $k_{\text{unfrozen,max}}$ [W m$^{-1}$ K$^{-1}$] | 0.48–1.50 | Calibrated: 0.631 | Deep thawed conductivity |
| depth_constant_k [m] | 0.5–2.0 | Calibrated: 1.396 | Conductivity transition depth |
| $C_{\text{frozen}}$ [J m$^{-3}$ K$^{-1}$] | $1.47\times10^6$–$2.21\times10^6$ | Calibrated: $1.574\times10^6$ | Frozen volumetric heat capacity |
| $C_{\text{unfrozen}}$ [J m$^{-3}$ K$^{-1}$] | $2.24\times10^6$–$3.36\times10^6$ | Calibrated: $3.104\times10^6$ | Thawed volumetric heat capacity |
| $g_{\text{geo}}$ [K m$^{-1}$] | 0.020–0.030 | Calibrated: 0.0204 | Lowell and Rona (2005) |

https://doi.org/10.5194/egusphere-2026-2371
Preprint. Discussion started: 18 June 2026


### 3.5.2 Coupled model

We utilized the same physically-constrained, minimal-parameter calibration strategy employed for the thermal component of Arctic-XBeach for the coupled component. Most hydrodynamic and morphodynamic parameters in XBeach were left at their validated default values (Roelvink et al., 2009) that have been extensively tested for a wide variety of coastal environments. The primary calibration effort focused on the parameters that (1) are highly variable at specific sites, (2) have a significant impact on the interactions between the thermal and morphodynamic processes, or (3) are responsible for mobilizing sediment on permafrost bluffs in Arctic coastal areas, where default parameterizations may not be applicable.

Based on their physical relevance to the processes driving coastal erosion in the Arctic, the following parameters were chosen to be optimized:

1. **Wave-driven transport asymmetry** (keyword `facua`): This parameter determine the contributions of wave skewness and wave asymmetry to onshore sediment transport. In XBeach, smaller values reduce the amount of onshore sediment transport and allow for more storm-driven offshore sediment transport. Asymmetry values in XBeach can range between 0 and 0.5.

2. **Bed friction coefficient** (keyword `bedfriccoef`): The Manning roughness coefficient determines the amount of energy lost by swash and overwash. Arctic beaches can be made up of poorly sorted sediment that can have significantly different roughness characteristics. Roughness values in the range 0.015–0.40.

3. **Avalanching slopes** (keyword `wetslp` and `dryslp`). These two parameters represent the maximum stable slope that can exist for wet and dry material. Once local slopes become greater than these two values, XBeach will redistribute sediment down the slope using an avalanching algorithm. For permafrost bluffs, the dry slope is particularly important since it represents the rate at which thawed material slumps from the bluff face onto the beach. The calibration range for this parameter, between 0.5 and 1.0, corresponds to the large variation in bluff face angles that have been measured at Arctic sites—dependent upon ice content and soil cohesion.

We again ran the Optuna hyperparameter optimization tool (Akiba et al., 2019) to find the combination of the calibrated sediment transport parameters that minimized the overall RMSE between the predicted and observed shoreline and bluff edge positions for Period 2 (2012–2015). This time period was selected for calibration due to the large variability in erosion rates during this interval, which represents a challenging test of the model's capability to simulate both the periods of active erosion and periods of quiescence. Each of the 200 trials consisted of a four-year coupled simulation plus 10-years for thermal spinup. The best parameter combination produced a combined RMSE of 4.1 m for Period 2, with bluff RMSE = 3.3 m and shoreline RMSE = 4.8 m (see Table 2). Convergence was confirmed by comparing the best objective values at 100 and 200 trials, which showed limited additional skill improvement beyond 100 trials.

https://doi.org/10.5194/egusphere-2026-2371
Preprint. Discussion started: 18 June 2026


**Table 2.** Coupled model parameters: fixed XBeach defaults and calibrated site-specific properties. Only parameters marked as "Calibrated" were varied during optimization; all others were held at default or physically constrained values.

| Parameter | Value / Range | Status | Rationale |
|---|---|---|---|
| *Fixed parameters (XBeach defaults or constrained)* | | | |
| $D_{50}$ [m] | $3.6 \times 10^{-5}$ | Fixed | Measured bluff sediment |
| morfac [−] | 1 | Fixed | No morphological acceleration (thermal coupling) |
| lsgrad [−] | 0 | Fixed | 1D model (no alongshore transport) |
| $N_{\text{thaw\_threshold}}$ [−] | 3 | Fixed | Minimum thawed cells |
| *Calibrated parameters (site-specific)* | | | |
| facua [−] | 0.00–0.40 | Calibrated: 0.019 | Wave skewness transport |
| bedfriccoef [$\text{s m}^{-1/3}$] | 0.015–0.035 | Calibrated: 0.034 | Manning bed friction |
| wetslp [−] | 0.05–0.30 | Calibrated: 0.152 | Wet critical slope |
| dryslp [−] | 0.50–1.00 | Calibrated: 0.558 | Dry critical slope |
| xb-threshold [−] | 2.0–2.5 | Calibrated: 2.01 | Runup activation threshold |

# 4 Results

## 4.1 Thermal Model Performance

### 4.1.1 Verification Against Analytical Solutions

In order to verify the thermal solver in Arctic-XBeach, we compared our model outputs to those obtained using the exact analytical solutions for three different heat conduction problems presented in Figure 5. In each case, the thermal properties were assumed to be homogeneous and constant across the domain with a constant thermal conductivity and constant volumetric heat capacity as a function of depth. We also assumed there was no geothermal gradient and that the initial conditions allowed us to maintain a single phase, which means that the enthalpy formulation reduced to linear heat diffusion and the analytical solutions can be directly applied. The three test cases are:

1. **Dirichlet warming**: A column of frozen soil, initially at 250 K, was warmed uniformly by a surface temperature of 270 K. For this case, we used the thermal properties of frozen soil: $k = 2.7$ W/m-K, $C = 4.6 \times 10^6$ J/m$^3$-K. The thermal diffusivity is therefore $\alpha = 5.87 \times 10^{-7}$ m$^2$/s, giving a characteristic penetration depth of $\sqrt{\alpha t} \approx 4.3$ m after 1 yr. The numerical solution follows very closely the analytical profile.

2. **Dirichlet cooling**: An unfrozen soil column, initially at 300 K, was cooled uniformly by setting a surface temperature of 280 K. As expected, because the thermal diffusivity of unfrozen soil ($\alpha = 8.57 \times 10^{-8}$ m$^2$/s, using $k = 0.6$ W/m-K and $C = 7.0 \times 10^6$ J/m$^3$-K) is much smaller than that of frozen soil, it takes much longer for heat to propagate through the domain and the penetration depth is much shallower. After 1 yr, the penetration depth is only $\sqrt{\alpha t} \approx 1.6$ m. In fact,

https://doi.org/10.5194/egusphere-2026-2371
Preprint. Discussion started: 18 June 2026


the penetration depth is about 7 times shallower than the penetration depth of frozen soil at the same time period. This is illustrated well in the middle panel of Figure 5.

3. **Neumann constant flux**: A constant heat flux of 5 W/m$^2$ was applied to the surface of a column of frozen soil that had been warmed to 250 K. However, unlike the previous two test cases, no surface temperature was specified. Instead, the surface temperature evolved freely in response to the flux applied to it. Therefore, the analytical solution for a semi-infinite medium (Carslaw, H. S. and Jaeger, 1959) was included as well.

Our numerical solutions for all three test cases match the analytical solutions well. The Neumann case provides the most stringent test of the flux boundary condition implementation and resulted in root-mean-square errors of less than 0.015 K for the entire simulation period (one year), with maximum errors of 0.05 K developing only in the final timestep when finite-domain effects become marginally detectable. These results verify that the enthalpy-based thermal solver correctly solves both Dirichlet-type (temperature) and Neumann-type (flux) surface boundary conditions and accurately captures diffusive heat transport for the full range of thermal property values representative of frozen and unfrozen permafrost soils. Following GMD conventions, we use verification to refer to demonstrating that the governing equations are solved correctly (this subsection), and evaluation to refer to demonstrating that the model adequately represents the observed system (subsequent subsections).

#### 4.1.2 Temperature Evaluation

Validation of the thermal component was performed by running the calibrated parameter set without additional tuning and comparing results to the independent 2011 data record from 2011-07-01 to 2011-10-01 (excluding the short-duration sensor malfunction; see section 3.3.1). The thermal component reproduced the observed seasonal temperature increase and the downward progression of this warm trend through the soil layers, with expected amplitude dampening and lower temperature values as one proceeds down into the soil.

The comparison between model and observation for the time-series at both the surface sensor (uppermost layer) and at $2\,\mathrm{m}$ depth showed good agreement. The RMSE of the uppermost layer comparison was $0.52\,^{\circ}\mathrm{K}$ and the mean bias of the model compared to the observations was $+0.34\,^{\circ}\mathrm{K}$ (model warmer than observed). The RMSE at the lower depth of 2 meters, was $1.70\,^{\circ}\mathrm{K}$, while the mean bias of the model compared to the observations was $-1.67\,^{\circ}\mathrm{K}$ (model cooler than observed). The time-evolution and vertical distribution of the warming signal are illustrated in Figure 6. The total RMSE for all data points included in the validation process indicated that the model had an error of $1.50\,^{\circ}\mathrm{K}$ and a mean bias of $-1.02\,^{\circ}\mathrm{K}$ (model cooler than observed).

### 4.2 Coupled Model Performance

The coupled Arctic-XBeach model was evaluated using shorelines and bluff data for Periods 1 and 3, neither of these time intervals was used for model calibration. In addition to showing the temporal development of both the observed and simulated coastal positions across each of the three evaluation periods, Figure 7 presents the temporal evolution of modeled and observed coastal positions across all three evaluation periods.

https://doi.org/10.5194/egusphere-2026-2371
Preprint. Discussion started: 18 June 2026


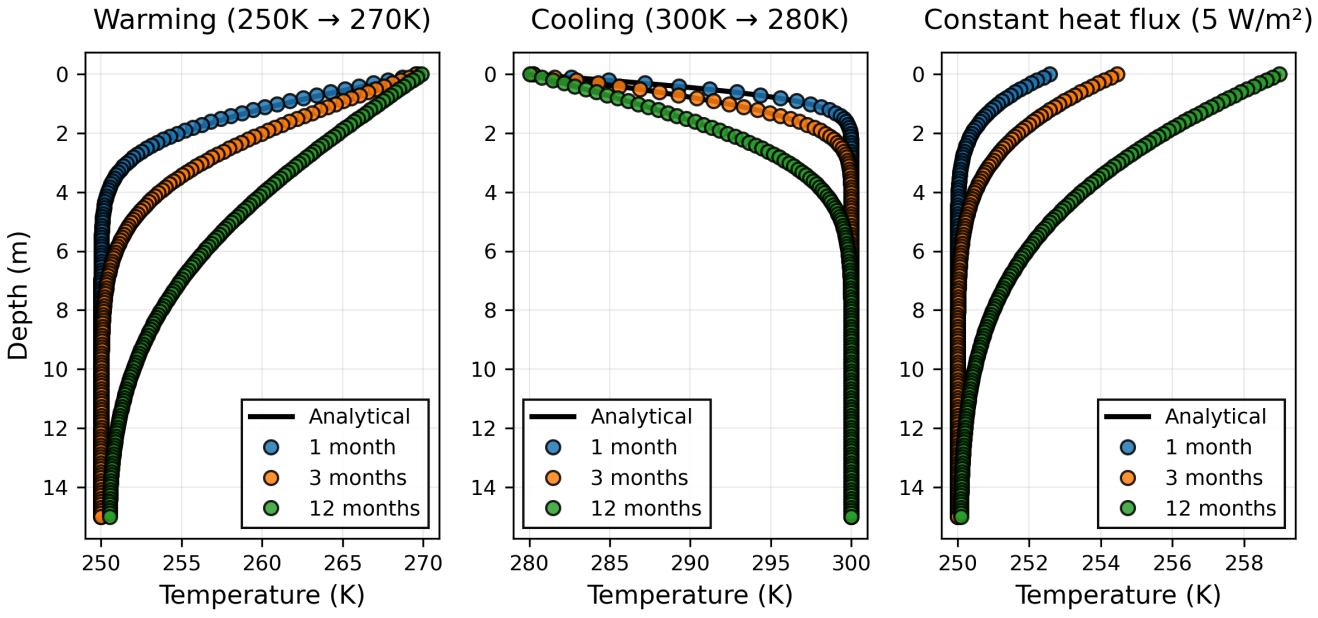


**Figure 5.** Comparison of analytical solutions to the thermal solver's results for the three test cases: (left) Dirichlet warming of a frozen soil column from 250 K to 270 K surface temperature, (middle) Dirichlet cooling of an unfrozen soil column from 300 K to 280 K surface temperature, and (right) constant Neumann heat flux of 5 W/m$^2$ applied to a frozen soil column. Solid black lines represent the analytical solutions. Colored markers represent the numerical solutions for each test case at 1 month, 3 months and 1 yr. The shallow penetration depth seen in the middle panel illustrates the lower thermal diffusivity of unfrozen soil.

The first period we evaluated was the 2009–2011 period. During this validation period, there was lower than average wave energy, and less than one third of the year was free of ice cover, leading to very little observed erosion (bluff retreat of 0.4 m, shoreline retreat of 7.7 m). The model captured the shoreline retreat reasonably well (modeled 6.1 m vs. observed 7.7 m), but overestimated bluff retreat (modeled 7.7 m vs. observed 0.4 m; bluff RMSE = 4.8 m, bias = +3.9 m). This overestimation suggests that Arctic-XBeach avalanches too much bluff material during quiet periods when little wave activity exists to remove slumped material from the base of the bluff, potentially due to overestimation of temperature and/or radiation. The combined RMSE for the period was 4.1 m.

The second period evaluated is the calibration period 2012–2015, which contained the highest erosion rates in the observation record (15.0 m of bluff retreat and 17.3 m of shoreline retreat over three years). The model reproduced the bluff retreat trend well (modeled 14.1 m; bluff RMSE = 3.3 m, bias = −2.5 m) but underestimated shoreline retreat (modeled 9.4 m; shoreline RMSE = 4.8 m, bias = −1.6 m). The combined RMSE for the calibration period was 4.1 m.

The last period evaluated is the 2016–2018 validation period, during which erosion was continuous with 7.9 m of observed bluff retreat and 16.1 m of observed shoreline retreat. The model captured the bluff erosion trend well (modeled 9.9 m vs.

https://doi.org/10.5194/egusphere-2026-2371
Preprint. Discussion started: 18 June 2026


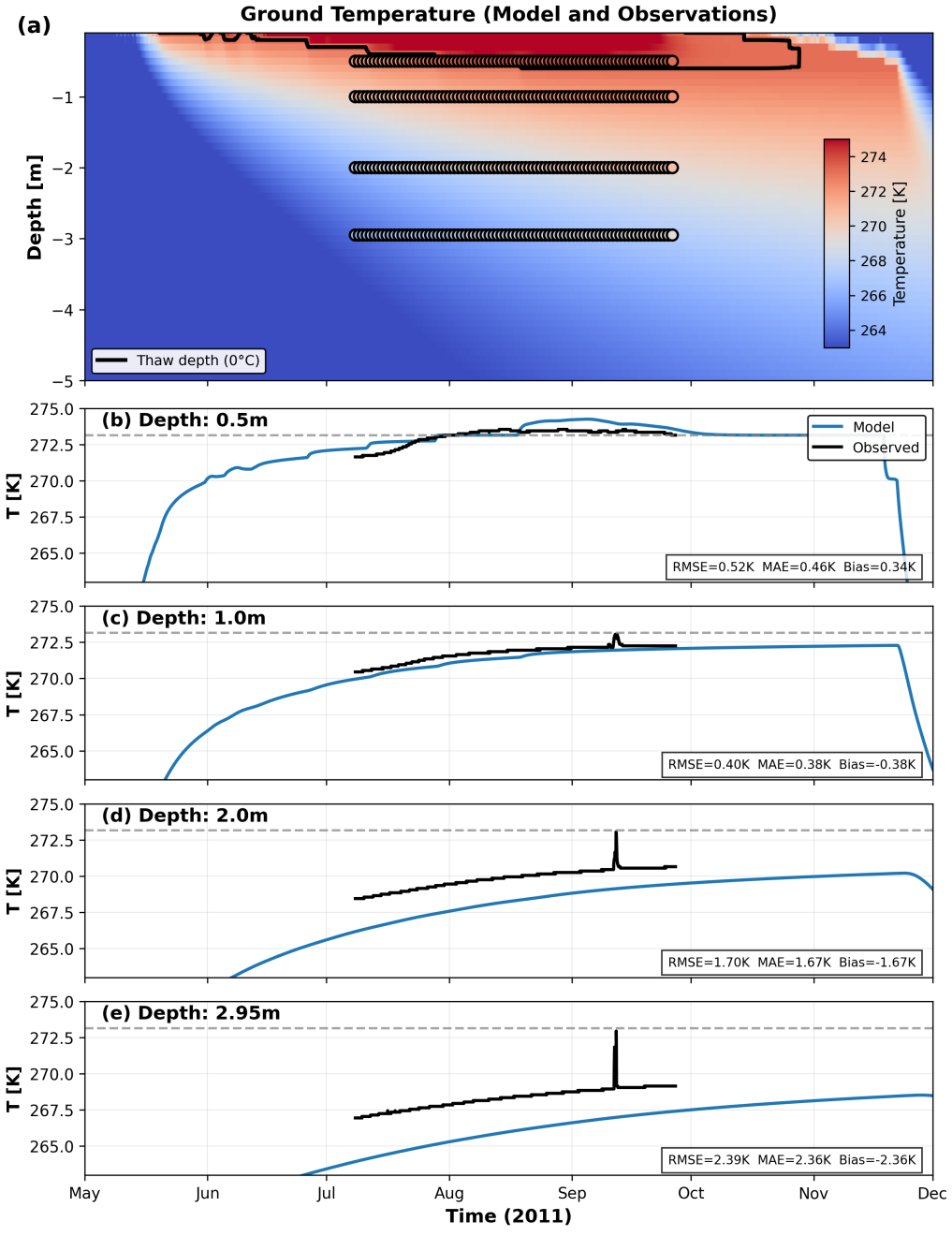


**Figure 6.** Model validation of subsurface ground temperature dynamics for May–December 2011. (a) Depth–time evolution of modeled ground temperature (color scale) with observed sensor measurements (circles) at approximately 0.5, 1.0, 2.0, and 2.95 m depth. The black contour denotes the modeled thaw depth (0 °C isotherm), illustrating seasonal warming and downward propagation of heat. (b–e) Time series comparison between modeled (blue) and observed (black) temperatures at the respective depths. The dashed gray line indicates the freezing threshold (273.15 K). Statistical performance metrics (RMSE, MAE, and bias) are reported for each depth, demonstrating good agreement near the surface and increasing cold bias with depth.

https://doi.org/10.5194/egusphere-2026-2371
Preprint. Discussion started: 18 June 2026


observed 7.9 m; bluff RMSE = 1.3 m, bias = +1.1 m), though shoreline retreat was underestimated (modeled 6.2 m; shoreline RMSE = 2.5 m, bias = −1.8 m). The combined RMSE for this period was 2.0 m.

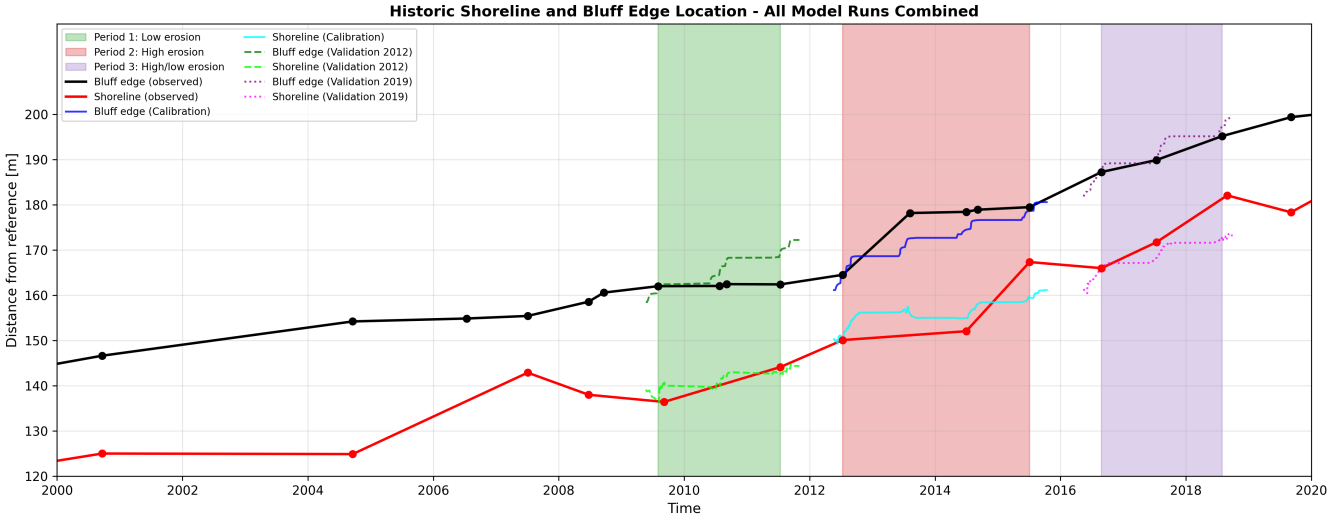


**Figure 7.** Modeled and observed shoreline and bluff-edge positions from 2000 to 2020. Observed bluff-edge and shoreline positions are shown by black and red lines, respectively. Solid black lines indicate modeled positions at the end of the calibration period (Period 2), while dashed and dotted black lines indicate modelled positions at the beginning and end of the validation period (Period 3; 2012 and 2019, respectively). Shaded regions denote the three evaluation periods: green for Period 1 (low erosion), red for Period 2 (calibration period, high erosion), and purple for Period 3 (validation period, variable erosion). Increasing distance from the reference point indicates landward retreat.

Overall, the coupled Arctic-XBeach model depicts multi-year erosion trends at Barter Island with a combined RMSE ranging from 2.0 to 4.1 m across the three evaluation periods. The model performed best during the high-erosion validation period (Period 3, RMSE = 2.0 m) and during calibration (Period 2, RMSE = 4.1 m). Performance was lower during the quiescent period (Period 1, RMSE = 4.1 m), where the small absolute retreat magnitudes amplify the relative error.

## 5 Discussion

### 5.1 Model performance

Arctic-XBeach pushes the boundaries of previous Arctic coastal models since it utilizes all aspects of XBeach physics and incorporates permafrost thermal dynamics into an open-source, modular Python framework. Unlike previous implementations of permafrost thermal and hydrodynamic-morphodynamic couplings using Fortran (Ravens et al., 2023), our implementation is modular, allowing the thermal and hydrodynamic-morphodynamic modules to operate independently except through the exchange of thaw depth, thus facilitating maintenance and future additions.

https://doi.org/10.5194/egusphere-2026-2371
Preprint. Discussion started: 18 June 2026


Compared to ArcticBeach v1.0 (Rolph et al., 2022) and the XBeach submodule approach of Islam and Lubbad (2022), our approach clearly decouples thermal and morphodynamic time steps for computational efficiency. The thermal module is run at sub-hourly time-steps to capture the temporal variability of heat diffusion and phase-change dynamics, while XBeach is only run when storm conditions occur with sufficient thawed sediment to prevent excessive computational requirements, representing an event-driven approach suitable for simulating timescales ranging from years to decades with modest computational costs. These efficiencies are necessary to support multi-decadal climate change projections (Nielsen et al., 2022).

The formulations utilized in Arctic-XBeach employ an enthalpy-based treatment of the phase transition zone to maintain numerical stability when approaching the melting point (Frederick et al., 2021). Analytical validation against the Carslaw, H. S. and Jaeger (1959) solution shows that Arctic-XBeach accurately represents both Dirichlet and Neumann boundary conditions in steady-state constant forcing scenarios.

The use of an event-driven coupling strategy in Arctic-XBeach produces substantial reductions in computational cost as opposed to using continuous coupling. Because XBeach runs only during storm events when thawed sediment is available (and not continuously), the computational cost is reduced by >99% compared to continuous coupling. The reason for this reduction in computational time is the episodic nature of Arctic coastal erosion. Sea ice essentially eliminates wave forcing for approximately nine months out of each year, and only a limited number of open water storms occur, which produce enough run-up to allow thawed bluff material to be mobilized. At Barter Island, XBeach was only activated for between 3-5 days per simulated year versus the full 365 days for continuous coupling. Conversely, the computationally inexpensive thermal module was run continuously at sub-hourly intervals in order to track the evolution of the active layer. This architecture has allowed the authors to complete multi-decadal simulations within hours as opposed to weeks which has enabled the authors to perform both ensemble and sensitivity analyses.

The coupled Arctic-XBeach model accurately replicates the observed multi-year shoreline and bluff edge retreat at Barter Island. The total Root Mean Square Error (RMSE) of the modeled retreat was determined to be 2.0–4.1 meters over the three evaluation periods. The model performed best during periods of active erosion (periods 2 and 3) and accurately captured both the magnitude and timing of the retreat. During the relatively inactive period (period 1), the skill of the model was lower due to smaller absolute magnitudes of retreat, resulting in larger relative error. Whether the compensating biases between quiescent and active periods remain balanced over multi-decadal simulations warrants further investigation with longer continuous runs. This phenomenon is analogous to the signal-to-noise challenge in coastal morphodynamic modeling (Vitousek et al., 2017); when the rate of erosion is low, uncertainty in the forcing variables and the initial condition variables can have a larger impact on the modeled retreat, while during active erosion, the dominant processes controlling the retreat (i.e., sediment transport via wave action, thermally controlled sediment availability) are well characterized.

### 5.2 Applicability, assumptions and limitations

Arctic-XBeach was developed to simulate the thermal denudation erosion mechanism, where the gradual thawing of permafrost bluffs causes slumping and the subsequent removal of thawed sediment through wave action. The mechanism discussed above

https://doi.org/10.5194/egusphere-2026-2371
Preprint. Discussion started: 18 June 2026


is dominant at coastal locations with moderate bluff heights and gradual slopes, which represent the majority of the Alaskan Beaufort Sea coast (Lantuit et al., 2012; Jones et al., 2018).

The 1D thermal transect approach effectively determines vertical temperature profiles and thaw depths that ultimately determine sediment erodibility. However, this approach does not account for the influence of pore water salinity on the freezing point depression (Guimond et al., 2021), nor do the formulations explicitly represent ice wedge polygons that increase the weakness of blocks that fail (Hoque and Pollard, 2009; Kanevskiy et al., 2013). The 1D formulation is also unable to accurately capture the lateral heat flow near the base of steep bluff faces or thermal niches, which require at least 2DV temperature fields to resolve (Frederick et al., 2021). Additionally, vegetation and organic mats near the tundra surface can stabilize thawed soils and insulate the bluff face, processes not currently represented in the model. This may contribute to the overestimation of retreat during quiescent periods.

The thermal domain is set at 10 m depth. While the recommendation is to consider deeper domains (50 – 100 m) for century-scale climate projections (Romanovsky et al., 2010), the results from the sensitivity testing indicate that increasing the domain depth does not significantly affect thaw depths or temperature distributions in the upper 2 m of the active layer, where sediment erodibility is determined. Therefore, the 10 m domain is deemed adequate for the seasonal to decadal timescales being simulated here.

While XBeach is capable of modeling multiple grain sizes, the primary focus of the model validations have been for non-cohesive, sandy environments (Roelvink et al., 2009). However, many Arctic permafrost bluffs are comprised of cohesive, fine-grained sediments. Fine-grained permafrost sediments typically undergo rapid liquefaction upon thawing due to excess pore-ice content exceeding the liquid limit, resulting in a fundamental alteration in the mechanical behavior of these sediments (Are et al., 2008). In its current configuration, Arctic-XBeach does not account for the behavior of cohesive sediments and users are cautioned against applying the model to sites where cohesive sediments dominate. Additionally, cohesive sediments with high ice content can be indicative for the dominance of thermal abrasion (Ravens and Peterson, 2021), a process not included in the current version of the model. For our specific application at Barter Island, we assume constant sediment properties for sediment diameter ($D_{50}$) and grain density ($p_s$) throughout the domain. This assumption is based on the fact that there was no detailed sediment characterization data available for our study site and likely also for other Arctic sites. Sensitivity analysis indicated that model response is much more sensitive to thermal processes (thermal module on/off) than to grain size parameters, suggesting that sediment erodibility is primarily controlled by whether the sediment is frozen or thawed. Additionally, XBeach is run in 1D cross-shore mode, which does not enable the modeling of alongshore sediment transport processes that are critical for long-term shoreline evolution.

ERA5 reanalysis provides atmospheric forcing at approximately 30 km resolution, which may not resolve local meteorological variations, although ERA5 demonstrates reliable skill at Arctic coastal sites (Hersbach et al., 2020). Sea ice protects against wave action during much of the year. While the model suppresses XBeach activation when ice concentration exceeds a threshold, gradual transitions between ice-free and ice-covered conditions during shoulder seasons are not explicitly represented.

https://doi.org/10.5194/egusphere-2026-2371
Preprint. Discussion started: 18 June 2026


### 5.3 Comparison to other models

Several models have addressed thermal abrasion, which involves wave-induced undercutting, creating thermo-erosional niches that destabilize the bluffs. Analytical solutions for the growth of these niches were presented by Kobayashi (1985) and incorporated into a process-based model by Ravens et al. (2012) for Drew Point. Barnhart et al. (2014) extended this process-based model and incorporated bluff stability concepts from Hoque and Pollard (2009), and simulated episodic erosion observed in time-lapse imagery. A new 3D finite element analysis was presented by Frederick et al. (2021). Most recently, Bayat et al. (2026) presented the Arctic Coastal Erosion Model (ArcEM) with a detailed calibration at Drew Point, Alaska.

The fully coupled model proposed by Islam and Lubbad (2022), was able to model thermo-denudation as well as thermoabrasion using sub-models representing thawing, slumping, niche growth, and bluff collapse. Some key differences between the two are: (1) the thermal zone representation is much simplified compared to our approach, where we model temperature through enthalpy; (2) we represent thermal state over timescales of years to decades allowing thaw depth to be representative of cumulative heat exchange; and (3) Arctic-XBeach is open source and licensed under the GPL-3.0 license allowing users to reproduce results and develop upon the code. By utilizing XBeach, a widely adopted nearshore modeling framework with an international user and developer base, Arctic-XBeach significantly lowers the barrier for coastal modelers to include permafrost processes in their studies without requiring knowledge of highly specific and complex Arctic erosion codes.

Lastly, Rolph et al. (2022) developed ArcticBeach v1.0 as a simple parametrization for a pan-arctic scale application within earth system models, with a focus on computational efficiency at the cost of process detail and generality. Arctic-XBeach provides a middle ground between very detailed, and thus computationally expensive, 3D models that are typically site-specific and very simple parametrizations that are computationally efficient but lacking physics; the event driven coupling allows for multi-decadal simulations while preserving physical realism.

### 5.4 Future development

Arctic-XBeach has been placed between high-resolution thermo-mechanical models and large-scale parameterizations of the entire Arctic Ocean, and many possible future developments can be derived from the limitations outlined above. We will outline the most likely future directions.

First of all, the convective heat transfer coefficient for the soil-water interface is assumed to be constant. A velocity-dependent formulation of this heat transfer coefficient using the scaling laws of a turbulent boundary layer (e.g., $h_c \propto u_{\mathrm{rms}}^{0.8}$) could be readily implemented into the existing structure of the model. This would allow the model to simulate variable heat transfer coefficients both spatially and temporally within storms, and may improve the simulation of thermal erosion in the swash and surf zones.

Second, an extension of the thermal model from 1D to 2D would solve at least some of the problems mentioned above. For example, lateral heat exchange in areas with steep bluff faces, salinity effects on the depression of the freezing point (Guimond et al., 2021), and heterogeneous ground-ice structures (Kanevskiy et al., 2013) could all be simulated in a 2DV version of the

https://doi.org/10.5194/egusphere-2026-2371
Preprint. Discussion started: 18 June 2026


model. An extension to 2DV would also provide a natural pathway to include a niche erosion module after Kobayashi (1985); allowing application to thermal-abrasion dominated locations that are currently out of the range of the model.

Third, the XBeach cross-shore configuration does not have the ability to simulate alongshore sediment transport, and thus cannot simulate the long-term evolution of shoreline morphology. To overcome this limitation, it would be necessary to couple Arctic-XBeach to larger-scale regional morphodynamic models (such as Delft3D (Lesser et al., 2004)). In this way, Arctic-XBeach would calculate local cross-shore erosion rates and sediment transport rates, while Delft3D would simulate longer-term alongshore sediment transport and shoreline migration. For many coastal communities, sediment supplied from eroding bluffs supplies downdrift beaches that provide critical coastal protection; a coupling of Arctic-XBeach with a model such as Delft3D would therefore be highly beneficial for these communities.

Fourth, it is estimated that Arctic coastal erosion is releasing 5–14 Tg C $yr^{-1}$from around the Arctic Ocean (Wegner et al., 2015) and this rate is expected to increase by a factor of two before the end of the century (Nielsen et al., 2022). The volume of erosion calculated by Arctic-XBeach could therefore be used to estimate carbon fluxes, thereby providing a mechanistic link between coastal erosion and the release of organic carbon that is missing from most Earth System Models.

Finally, the event-driven initiation strategy includes sensitivities to user-defined thresholds for run-up, sea-ice concentration and the time period between storms. Currently, sea-ice is treated as being solely protective, whereas there are many other ways in which sea-ice influences the nearshore environment, including scouring and sediment transport by shore-fast ice (Theuerkauf et al., 2024). Incorporating these processes into Arctic-XBeach would improve the model's representation of shoulder season processes. Improved boundary conditions could be achieved through downscaling ERA5 with regional atmospheric and spectral wave models that account for sea-ice processes (Rogers, 2019; Nederhoff et al., 2020), which would reduce the model's sensitivity to user-defined thresholds.

### 5.5 Societal relevance

In terms of societal relevance, Arctic coastal erosion poses many risks to indigenous peoples, as well as to both their physical and cultural infrastructure. Alaska Native Tribal Health Consortium (ANTHC), there are approximately 144 Native communities that exist under threat from coastal erosion and/or flooding and/or melting of permafrost in Alaska, with at least 31 being directly in harm's way (ANTHC (Alaska Native Tribal Health Consortium), 2024). Many communities have already begun to implement solutions such as relocation and protective measures; however, due to the costs associated with these efforts, they will likely continue to face challenges in this area (U.S. Government Accountability Office (GAO), 2009). Furthermore, when considering compound effects of erosion, subsidence, and rising sea levels, it has been estimated that there will be an increase of 6-8 fold in the amount of land turned to sea due to erosion alone by 2100 (Creel et al., 2024). As such, the ability to make decisions through use of physically-based, coupled thermal – morphological process-based erosion predictions will assist in decision-making to protect arctic coastal communities and infrastructure. The event-driven approach to modeling arctic erosion events as well as the models ability to assess future risk trajectories based upon multiple climate scenarios will also help provide insight into the potential for long-term changes in arctic coastal hazards. By providing free access to the model, we

https://doi.org/10.5194/egusphere-2026-2371
Preprint. Discussion started: 18 June 2026


hope to aid researchers and practitioners working on behalf of government agencies, private consulting firms, and community planning organizations who are working to protect arctic coastal communities and infrastructure.

## 6 Conclusions

Arctic-XBeach is a new coupled thermo-morphodynamic model for simulating the evolution of permafrost coastlines. We created Arctic-XBeach using existing codes for simulating arctic coastal erosion written in a Python framework. Through this process, we were able to create a modular integration of an XBeach-based hydrodynamic model with a 1D heat transfer (freeze-thaw) model. The governing equations used in this model consist of the shallow water and Exner sediment equations for the XBeach model, and a 1D diffusion (enthalpy) equation for soil temperatures. The coupling strategy used in this model consists of using the active thaw depth to update an erodibility mask within the XBeach model, which allows only thawed soil to be mobilized by waves. To improve computational efficiency, we developed a new computational workflow that alternates between updating the thermal conditions and running select storm-driven XBeach simulations. We tested the Arctic-XBeach model using a case study of Barter Island (US) and successfully reproduced the expected seasonal erosion patterns. The methodology employed in this paper enables the prediction of coastal change over climate-relevant time scales and can be applied to other arctic sites, provided the necessary background information and calibration data are available. The Arctic-XBeach code was made available online through Zenodo and GitHub, and we plan to extend this work in the near term by incorporating alongshore dynamics, more complex failure processes such as thermal abrasion, and by developing regional sea ice projections.

*Code availability.* The Arctic-XBeach code is freely available to anyone and published on Zenodo (10.5281/zenodo.19736549 or Nederhoff et al. (2026)) and GitHub (https://github.com/Deltares-research/arctic-xbeach, last access: April 24, 2026).

*Data availability.* The ERA5 climate reanalysis that was used to provide the climate forcing for the simulation is also available from the European Centre for Medium-Range Weather Forecasts (ECMWF). The source of the bluffs and shoreline elevation at Barter Island, as well as the source of the soil temperature measurements used in this study, are provided and other input data required to run the model for the Barter Island site can be found in the citations listed for each relevant section or can be obtained directly from the authors as part of the code package release.

## Appendix A: Solar Calculator

The radiation flux is the sum of the net influx of shortwave and longwave radiation (Equation A1).

$$q_{\text{radiation}} = q_{\text{radiation, shortwave}} + q_{\text{radiation, longwave}} \tag{A1}$$

https://doi.org/10.5194/egusphere-2026-2371
Preprint. Discussion started: 18 June 2026


The shortwave radiation flux on a surface depends on the angle that the incoming radiation makes with that surface. Shortwave radiation heat flux data are available for flat surfaces. However, data are not available for an inclined surface (such as a permafrost bluff). To account for bluff inclination, we used a 'solar flux calculator' to scale radiation from a flat surface to an inclined surface (Kasper et al., 2023). For an inclined surface, the amount of incoming radiation was determined using Equation A2 (Buffo et al., 1972).

$$I = I_0 p^{1/\sin A} \sin\theta \tag{A2}$$

where,

$I$ = solar intensity [W/m$^2$] (equals $q_{\text{radiation, shortwave}}$ in Equation A1),

$I_0$ = solar constant [W/m$^2$] (radiation at the top of the atmosphere normal to the sun),

$p$ = atmospheric transmission coefficient (depending on altitude, weather, etc.),

$A$ = altitude angle [°] (angle off of the horizontal with which the sun's rays strike a horizontal surface),

$\phi$ = latitude [°],

$\delta$ = declination angle [°] $= 23.5 \times \frac{2\pi}{360} \cos \frac{2\pi}{365}(284 + N)$,

$N$ = current day of the year [-],

$h$ = hour angle [°] (varies daily, equaling 0 at 12:00 and $\pi$ at 00:00, local time),

$\theta$ = angle between surface and radiation [°] $= \sin A \cos\alpha - \cos A \sin\alpha \sin Z - \beta$,

$Z$ = azimuth counter-clockwise from east [°] = $AZ + \frac{1}{2}\pi$,

$AZ$ = azimuth counter-clockwise from south [°] = $\arcsin \cos\delta \frac{\sin h}{\cos A}$,

Near the solstices, the sun sometimes crosses the east-west line. This happens when $\cos h < \frac{\tan\delta}{\tan\phi}$. If this condition is satisfied, the equation for $AZ$ is modified through Equation A3.

$$AZ = \begin{cases} -\pi + |AZ|, & h < 0 \text{ (before 12:00)} \\ \pi - AZ, & h > 0 \text{ (after 12:00)} \end{cases} \tag{A3}$$

The shortwave solar radiation data we used to force the model is defined on the Earth's surface for zero inclination. Equations A4 and A5 respectively represent the intensity of solar radiation on a flat surface, $I_{\text{flat}}$, and intensity of solar radiation on an inclined surface, $I_{\text{inclined}}$.

https://doi.org/10.5194/egusphere-2026-2371
Preprint. Discussion started: 18 June 2026


$$I_{\text{flat}} = I_0 p^{1/\sin A} \sin\theta_{\text{flat}} \tag{A4}$$

$$I_{\text{inclined}} = I_0 p^{1/\sin A} \sin\theta_{\text{inclined}} \tag{A5}$$

The atmospheric transmission coefficient is not affected by surface inclination. Hence, we related $I_{\text{flat}}$ and $I_{\text{inclined}}$ through Equation A6.

$$I_{\text{inclined}} = I_{\text{flat}} \frac{\sin\theta_{\text{inclined}}}{\sin\theta_{\text{flat}}} = I_{\text{flat}} r \tag{A6}$$

where,

$r$ = enhancement factor.

We used Equation A6 to compute the intensity of shortwave radiation on an inclined surface based on the intensity of shortwave radiation on a flat surface. The enhancement factor $r$ is a function of surface inclination, day of the year, latitude, etc. (Equations A2 - A5).

We conclude that solar radiation on a north-facing (positively) inclined surface should be reduced for most of the year. Conversely, a negative slope (i.e., a south-facing bluff) leads to a more perpendicular angle between incoming radiation and the surface. This means rays of solar radiation are distributed over a smaller area, which relates to higher solar intensity, and hence an enhancement factor larger than one.

*Author contributions.* KN led the writing, model integration, and case study analysis. KdB rewrote Arctic-XBeach in Python, developed the thermal module, and performed the Barter Island case study. TR initiated the Arctic-XBeach concept and developed the original Fortran-based version. CS supported coupling, validation, and project coordination. SP contributed to the model formulation and manuscript preparation. RM provided guidance on XBeach implementation and coupling strategy. LE supplied observational data, contributed to forcing data development, and supported model evaluation. FO provided the 2016 thermal calibration data and contributed to the site characterization. All authors contributed to discussions and final manuscript revisions.

*Competing interests.* The contact author has declared that none of the authors has any competing interests

*Disclaimer.* Any use of trade, firm, or product names is for descriptive purposes only and does not imply endorsement by the U.S. Government

https://doi.org/10.5194/egusphere-2026-2371
Preprint. Discussion started: 18 June 2026


*Acknowledgements.* We acknowledge the Deltares SITO-IS research funding as part of the Moonshot 2 – Flooding project, which has provided funding to develop the model and write this paper. We also thank Bay Berry and Emily Bristol for their critical review, which improved the manuscript.

https://doi.org/10.5194/egusphere-2026-2371
Preprint. Discussion started: 18 June 2026


## References

Akiba, T., Sano, S., Yanase, T., Ohta, T., and Koyama, M.: Optuna: A Next-generation Hyperparameter Optimization Framework, in: Proceedings of the 25th ACM SIGKDD International Conference on Knowledge Discovery & Data Mining, ACM, https://doi.org/10.1145/3292500.3330701, 2019.

ANTHC (Alaska Native Tribal Health Consortium): Unmet Needs of Environmentally Threatened Alaska Native Villages: Assessment and Recommendations, 2024.

Are, F., Reimnitz, E., Grigoriev, M., Hubberten, H., and Rachold, V.: The Influence of Cryogenic Processes on the Erosional Arctic Shoreface, Journal of Coastal Research, pp. 110–121, https://doi.org/10.2112/05-0573.1, 2008.

Barnhart, K. R., Anderson, R. S., Overeem, I., Wobus, C., Clow, G. D., and Urban, F. E.: Modeling erosion of ice-rich permafrost bluffs along the Alaskan Beaufort Sea coast, Journal of Geophysical Research: Earth Surface, 119, 1155–1179, https://doi.org/10.1002/2013JF002845, 2014.

Bayat, A., Bulls, C., and Ravens, T. M.: The Arctic Coastal Erosion Model: Overview, Developments, and Calibration at Drew Point, Alaska, Journal of Advances in Modeling Earth Systems, 2026.

Buffo, J., Fritschen, L. J., and Murphy, J. L.: Direct Solar Radiation on Various Slopes from 0 to 60 Degrees North Latitude, Research Paper PNW-142, USDA Forest Service, Pacific Northwest Forest and Range Experiment Station, 1972.

Bull, D., Bristol, E., Brown, E., Choens, R., Connolly, C., Flanary, C., Frederick, J., Jones, B., Jones, C., Ward Jones, M., McClelland, J., Mota, A., and Tezaur, I.: Arctic Coastal Erosion: Modeling and Experimentation, pp. 1–270, https://doi.org/10.2172/1670531, 2020.

Carslaw, H. S. and Jaeger, J. C.: Conduction of Heat in Solids, Oxford University Press, 2nd edn., 1959.

Coco, A., Currenti, G., Del Negro, C., and Russo, G.: A second order finite-difference ghost-point method for elasticity problems on unbounded domains with applications to volcanology, Communications in Computational Physics, 16, 983–1009, https://doi.org/10.4208/cicp.210713.010414a, 2014.

Creel, R., Guimond, J., Jones, B. M., Nielsen, D. M., Bristol, E., Tweedie, C. E., and Overduin, P. P.: Permafrost thaw subsidence, sea-level rise, and erosion are transforming Alaska's Arctic coastal zone, Proceedings of the National Academy of Sciences (PNAS), 121, 1–7, https://doi.org/10.1073/pnas.2409411121/-/DCSupplemental.Published, 2024.

Engelstad, A. C., Erikson, L. H., Reguero, B. G., Gibbs, A. E., and Nederhoff, K.: Nearshore wave time-series along the coast of Alaska computed with a numerical wave model,, USGS Data Release, https://doi.org/https://doi.org/10.5066/P931CSO9, 2024.

Erikson, L., Gibbs, A. E., Richmond, B. M., Jones, B. M., Storlazzi, C. D., and Ohman, K.: Modeled 21st century storm surge, waves, and coastal flood hazards and supporting oceanographic and geological field data (2010 and 2011) for Arey and Barter Islands, Alaska and vicinity, https://doi.org/10.5066/P9LGYO2Q, 2020a.

Erikson, L., Gibbs, A. E., Richmond, B. M., Storlazzi, C. D., Jones, B. M., and Ohman, K. A.: Changing Storm Conditions in Response to Projected 21st Century Climate Change and the Potential Impact on an Arctic Barrier Island – Lagoon System — A Pilot Study for Arey Island and Lagoon , Eastern Arctic Alaska, USGS Open-File Report, https://doi.org/https://doi.org/10.3133/ofr20151193, 2020b.

Farouki, O. T.: Thermal properties of soils, Monograph Monograph 81-1, U.S. Army Corps of Engineers, Cold Regions Research and Engineering Laboratory (CRREL), Hanover, NH, 1981.

Foley, N., Tulaczyk, S., Oberle, F. K. J., Johnson, C. D., Swarzenski, P., Richmond, B. M., Gibbs, A., Erikson, L., and Lorenson, T.: Ground temperature data of Barter Island bluffs collected in 2016, https://doi.org/10.5066/P13OM8JN, data release, 2026.

https://doi.org/10.5194/egusphere-2026-2371
Preprint. Discussion started: 18 June 2026


Frederick, J., Mota, A., Tezaur, I., and Bull, D.: A thermo-mechanical terrestrial model of Arctic coastal erosion, Journal of Computational and Applied Mathematics, 397, 113 533, https://doi.org/10.1016/j.cam.2021.113533, 2021.

Gibbs, A. E. and Richmond, B.: National Assessment of Shoreline Change — Historical Shoreline Change Along the North Coast of Alaska, U.S .-Canadian Border to Icy Cape, U.S. Geological Survey Open-File Report 2015–1048, 96 p, 2015.

Gibbs, A. E., Erikson, L., Jones, B. M., Richmond, B. M., and Engelstad, A. C.: Seven decades of coastal change at barter island, alaska: Exploring the importance of waves and temperature on erosion of coastal permafrost bluffs, Remote Sensing, 13, https://doi.org/10.3390/rs13214420, 2021.

Goda, Y.: Random Seas and Design of Maritime Structures, WORLD SCIENTIFIC, 3rd edn., https://doi.org/10.1142/7425, 2010.

Guimond, J. A., Mohammed, A. A., Walvoord, M. A., Bense, V. F., and Kurylyk, B. L.: Saltwater Intrusion Intensifies Coastal Permafrost Thaw, Geophysical Research Letters, pp. 1–10, https://doi.org/10.1029/2021GL094776, 2021.

Hersbach, H., Bell, B., Berrisford, P., Hirahara, S., Horányi, A., Muñoz-Sabater, J., Nicolas, J., Peubey, C., Radu, R., Schepers, D., Simmons, A., Soci, C., Abdalla, S., Abellan, X., Balsamo, G., Bechtold, P., Biavati, G., Bidlot, J., Bonavita, M., De Chiara, G., Dahlgren, P., Dee, D., Diamantakis, M., Dragani, R., Flemming, J., Forbes, R., Fuentes, M., Geer, A., Haimberger, L., Healy, S., Hogan, R. J., Hólm, E., Janisková, M., Keeley, S., Laloyaux, P., Lopez, P., Lupu, C., Radnoti, G., de Rosnay, P., Rozum, I., Vamborg, F., Villaume, S., and Thépaut, J. N.: The ERA5 global reanalysis, Quarterly Journal of the Royal Meteorological Society, pp. 1–51, https://doi.org/10.1002/qj.3803, 2020.

Hoque, A. and Pollard, W. H.: Arctic coastal retreat through block failure, Canadian Geotechnical Journal, 1115, 1103–1115, https://doi.org/10.1139/T09-058, 2009.

Hoque, A. and Pollard, W. H.: Stability of permafrost dominated coastal cliffs in the Arctic, Polar Science, 10, 79–88, https://doi.org/10.1016/j.polar.2015.10.004, 2016.

Hu, H. and Argyropoulos, S. A.: Mathematical modelling of solidification and melting: A review, Modelling and Simulation in Materials Science and Engineering, 4, 371–396, https://doi.org/10.1088/0965-0393/4/4/004, 1996.

Irrgang, A. M., Bendixen, M., Farquharson, L. M., Baranskaya, A. V., Erikson, L. H., Gibbs, A. E., Ogorodov, S. A., Overduin, P. P., Lantuit, H., Grigoriev, M. N., and Jones, B. M.: Drivers, dynamics and impacts of changing Arctic coasts, Nature Reviews Earth & Environment, 3, 396–410, https://doi.org/10.1038/s43017-022-00260-5, 2022.

Islam, M. A. and Lubbad, R.: A Process-Based Model for Arctic Coastal Erosion Driven by Thermodenudation and Thermoabrasion Combined and including Nearshore Morphodynamics, Journal of Marine Science and Engineering, 10, https://doi.org/10.3390/jmse10111602, 2022.

Jones, B. M., Arp, C. D., Jorgenson, M. T., Hinkel, K. M., Schmutz, J. A., and Flint, P. L.: Increase in the rate and uniformity of coastline erosion in Arctic Alaska, Geophysical Research Letters, 36, 1–5, https://doi.org/10.1029/2008GL036205, 2009.

Jones, B. M., Farquharson, L. M., Baughman, C. A., Buzard, R. M., Arp, C. D., Grosse, G., Bull, D. L., Günther, F., Nitze, I., Urban, F., Kasper, J. L., Frederick, J. M., Thomas, M., Jones, C., Mota, A., Dallimore, S., Tweedie, C., Maio, C., Mann, D. H., Richmond, B., Gibbs, A. E., Xiao, M., Sachs, T., Iwahana, G., Kanevskiy, M., and Romanovsky, V. E.: A decade of remotely sensed observations highlight complex processes linked to coastal permafrost bluff erosion in the Arctic, Environmental Research Letters, 13, https://doi.org/10.1088/1748-9326/aae471, 2018.

Jones, B. M., Irrgang, A. M., Farquharson, L. M., Lantuit, H., Whalen, D., Ogorodov, S., Grigoriev, M., Tweedie, C., Gibbs, A. E., Strzelecki, M. C., Baranskaya, A., Belova, N., Sinitsyn, A., Kroon, A., Maslakov, A., Vieira, G., Grosse, G., Overduin, P., Nitze, I., Maio, C., Overbeck, J., Bendixen, M., Zagórski, P., and Romanovsky, V. E.: Arctic Report Card 2020: Coastal Permafrost Erosion, NOAA Arctic Report Card 2020, pp. 1–10, https://doi.org/10.25923/e47w-dw52, 2020.

https://doi.org/10.5194/egusphere-2026-2371
Preprint. Discussion started: 18 June 2026


Kanevskiy, M., Shur, Y., Jorgenson, M. T., Ping, C., Michaelson, G. J., Fortier, D., Stephani, E., Dillon, M., and Tumskoy, V.: Cold Regions Science and Technology Ground ice in the upper permafrost of the Beaufort Sea coast of Alaska, Cold Regions Science and Technology, 85, 56–70, https://doi.org/10.1016/j.coldregions.2012.08.002, 2013.

Kasper, J., Erikson, L., Ravens, T., Bieniek, P., Engelstad, A. C., Nederhoff, K., Duvoy, P., Fisher, S., Brown, E. P., Man, Y., and Reguero, B.: Central Beaufort Sea Wave and Hydrodynamic Modeling Study Report 1: Field measurements and model development, Report 1:, 2023.

Kobayashi, N.: Formation of Thermoerosional Niches into Frozen Bluffs due to Storm Surges on the Beaufort Sea Coast, Journal of Geophysical Research, https://doi.org/10.1029/JC090iC06p11983, 1985.

Kobayashi, N. and Aktan, D.: Thermoerosion of Frozen Sediment Under Wave Action, Journal of Waterway, Port, Coastal, and Ocean Engineering, 112, 140–158, https://doi.org/10.1061/(asce)0733-950x(1986)112:1(140), 1986.

Kobayashi, N., Vidrine, J., Nairn, R., and Solomon, S.: Erosion of Frozen Cliffs due to Storm Surge on Beaufort Sea Coast, Journal of Coastal Research, pp. 332–344, https://www.jstor.org/stable/4298946, 1999.

Lantuit, H., Overduin, P. P., Couture, N., Wetterich, S., Aré, F., Atkinson, D., Brown, J., Cherkashov, G., Drozdov, D., Forbes, D. L., Graves-Gaylord, A., Grigoriev, M., Hubberten, H.-W., Jordan, J., Jorgenson, T., Ødegård, R. S., Ogorodov, S., Pollard, W. H., Rachold, V., Sedenko, S., Solomon, S., Steenhuisen, F., Streletskaya, I., and Vasiliev, A.: The Arctic Coastal Dynamics Database: A New Classification Scheme and Statistics on Arctic Permafrost Coastlines, Estuaries and Coasts, 35, 383–400, https://doi.org/10.1007/s12237-010-9362-6, 2012.

Lesser, G. R., Roelvink, D., van Kester, J., and Stelling, G. S.: Development and validation of a three-dimensional morphological model, Coastal Engineering, 51, 883–915, https://doi.org/10.1016/j.coastaleng.2004.07.014, 2004.

Lowell, R. and Rona, P.: TECTONICS | Hydrothermal Activity, in: Encyclopedia of Geology, edited by Selley, R., Cocks, L., and Plimer, I., pp. 362–372, Elsevier, Oxford, ISBN 978-0-12-369396-9, https://doi.org/10.1016/B0-12-369396-9/00126-X, 2005.

Man, Y.: The Effect of Snow Deposition on Soil Temperature Profile in the Arctic, University of Alaska Anchorage ProQuest Dissertations & Theses, 2023.

Nairn, R. B. and Southgate, H. N.: Deterministic profile modelling of nearshore processes. Part 2. Sediment transport and beach profile development, Coastal Engineering, 19, 57–96, 1993.

Nairn, R. B., Solomon, S., Kobayashi, N., and Virdrine, J.: Development and Testing of a Thermal-Mechanical Numerical Model for Predicting Arctic Shore Erosion Processes, in: Permafrost: Proceedings of the Seventh International Conference, Yellowknife, NWT, June 23-27, pp. 789–795, Yellowknife, Canada, 1998.

Nederhoff, K.: Delft3D FM Alaska Tide and Storm Surge Model Output (1979–2022), https://doi.org/https://doi.org/10.5281/zenodo.15807568, 2025., 2025.

Nederhoff, K., Erikson, L., Engelstad, A., Bieniek, P., and Kasper, J.: Simulating the effects of climate change on waves in the nearshore of Foggy Island Bay, in: AGU Fall Meeting Abstracts, vol. 2020, pp. C003—-0016, 2020.

Nederhoff, K., Erikson, L., Engelstad, A., Bieniek, P., and Kasper, J.: The effect of changing sea ice on wave climate trends along Alaska's central Beaufort Sea coast, The Cryosphere, 16, 1609–1629, https://doi.org/10.5194/tc-16-1609-2022, 2022.

Nederhoff, K., de Bruijn, K., and Ravens, T.: Arctic-XBeach v1.0.0, https://doi.org/10.5281/zenodo.19736550, 2026.

Nielsen, D. M., Pieper, P., Barkhordarian, A., Overduin, P., Ilyina, T., Brovkin, V., Baehr, J., and Dobrynin, M.: Increase in Arctic coastal erosion and its sensitivity to warming in the twenty-first century, Nature Climate Change, 12, 263–270, https://doi.org/10.1038/s41558-022-01281-0, 2022.

https://doi.org/10.5194/egusphere-2026-2371
Preprint. Discussion started: 18 June 2026


Oberle, F. K. J., Johnson, C., Lorenson, T. D., Tan, A. C., and Richmond, B. M.: Grain size analysis and total carbon content of augered sediment samples from Barter Island, Alaska, https://doi.org/10.5066/P14FZKEF, data release, 2026.

Overduin, P. P., Strzelecki, M. C., Grigoriev, M. N., Couture, N., Lantuit, H., St-Hilaire-Gravel, D., Günther, F., and Wetterich, S.: Coastal changes in the arctic, Geological Society Special Publication, 388, 103–129, https://doi.org/10.1144/SP388.13, 2014.

Patankar, S. V.: Numerical Heat Transfer and Fluid Flow, Hemisphere Publishing Corporation, 1980.

Pearson, S. G., Lubbad, R., Le, T. M. H., and Nairn, R. B.: Thermo-mechanical Erosion Modelling using COSMOS: A case study at Baydaratskaya Bay, Russia, 8th International Conference on Scour and Erosion (ICSE 2016), Oxford, UK., 2016.

Ravens, T., Henke, M., and Ferreira, C. M.: ARCTIC COASTAL STORMS, UNIQUE IN CHARACTER AND IMPACT, Coastal Sediments 2023, pp. 2434–2461, https://doi.org/10.1142/9789811275135_0223, 2023.

Ravens, T. M. and Peterson, S.: Geologic Controls on Erosion Mechanism on the Alaska Beaufort Coast, 9, 1–8, https://doi.org/10.3389/feart.2021.693824, 2021.

Ravens, T. M., Jones, B. M., Zhang, J., Arp, C. D., and Schmutz, J. A.: Process-Based Coastal Erosion Modeling for Drew Point , North Slope , Alaska, pp. 122–131, https://doi.org/10.1061/(ASCE)WW.1943-5460.0000106., 2012.

Reimnitz, E. and Maurer, D. K.: Effects of Storm Surges on the Beaufort Sea Coast, Northern Alaska, Arctic, 32, 329–344, https://doi.org/10.14430/arctic2631, 1979.

Roelvink, D., McCall, R., Mehvar, S., Nederhoff, K., and Dastgheib, A.: Improving predictions of swash dynamics in XBeach: The role of groupiness and incident-band runup, Coastal Engineering, 134, 103–123, https://doi.org/10.1016/j.coastaleng.2017.07.004, 2018.

Roelvink, J., Reniers, A. J. H. M., Van Dongeren, A., van Thiel de Vries, J. S. M., McCall, R. T., Lescinski, J., Roelvink, D., Reniers, A. J. H. M., Van Dongeren, A., van Thiel de Vries, J. S. M., McCall, R. T., and Lescinski, J.: Modelling storm impacts on beaches, dunes and barrier islands, Coastal Engineering, 56, 1133–1152, https://doi.org/10.1016/j.coastaleng.2009.08.006, 2009.

Rogers, W. E.: Implementation of Sea Ice in the Wave Model SWAN, 2019.

Rolph, R., Overduin, P. P., Ravens, T., Lantuit, H., and Langer, M.: ArcticBeach v1.0: A physics-based parameterization of pan-Arctic coastline erosion, Frontiers in Earth Science, 10, 1–19, https://doi.org/10.3389/feart.2022.962208, 2022.

Romanovsky, V. E., Smith, S. L., and Christiansen, H. H.: Permafrost Thermal State in the Polar Northern Hemisphere during the International Polar Year 2007 – 2009 : a Synthesis, 116, 106–116, https://doi.org/10.1002/ppp.689, 2010.

Schaefer, K., Liu, L., Parsekian, A., Jafarov, E., Chen, A., Zhang, T., Gusmeroli, A., Panda, S., Zebker, H. A., and Schaefer, T.: Remotely Sensed Active Layer Thickness (ReSALT) at Barrow, Alaska Using Interferometric Synthetic Aperture Radar, Remote Sensing, 7, 3735–3759, https://doi.org/10.3390/rs70403735, 2015.

Stockdon, H. F., Holman, R. A., Howd, P. A., and Sallenger, A. H.: Empirical parameterization of setup, swash, and runup, Coastal Engineering, 53, 573–588, https://doi.org/10.1016/j.coastaleng.2005.12.005, 2006.

Swarzenski, P. W., Johnson, C. D., Lorenson, T. D., Conaway, C. H., Gibbs, A. E., Erikson, L. H., Richmond, B. M., and Waldrop, M. P.: Seasonal Electrical Resistivity Surveys of a Coastal Bluff, Barter Island, North Slope Alaska, Journal of Environmental and Engineering Geophysics, 21, 37–42, https://doi.org/10.2113/JEEG21.1.37, 2016.

Terhaar, J., Lauerwald, R., Regnier, P., Gruber, N., and Bopp, L.: Around one third of current Arctic Ocean primary production sustained by rivers and coastal erosion, Nature Communications, 12, 1–10, https://doi.org/10.1038/s41467-020-20470-z, 2021.

Theuerkauf, E., Zoet, L., Volpano, C., Dodge, S., Hartley, B., and Elmo Rawling, J.: Shore ice control on coastal geomorphic evolution in cold regions, Geomorphology, 466, 109 409, https://doi.org/10.1016/j.geomorph.2024.109409, 2024.

https://doi.org/10.5194/egusphere-2026-2371
Preprint. Discussion started: 18 June 2026


United States Census Bureau: 2020 Population and Housing State Data for Barter Island, AK. https://censusreporter.org/profiles/16000US0236990-kaktovik-ak/. Accessed 3 March 2026., https://censusreporter.org/profiles/16000US0236990-kaktovik-ak/, 2026.

U.S. Government Accountability Office (GAO): Alaska Native Villages: Limited Progress Has Been Made on Relocating Villages Threatened by Flooding and Erosion, 2009.

Vitousek, S., Barnard, P., Fletcher, C. H., Frazer, N., Erikson, L., and Storlazzi, C. D.: Doubling of coastal flooding frequency within decades due to sea-level rise, Scientific Reports, 7, 1–9, https://doi.org/10.1038/s41598-017-01362-7, 2017.

Wegner, C., Bennett, K. E., Vernal, A. D., Forwick, M., Fritz, M., Heikkilä, M., Łącka, M., Lantuit, H., Moskalik, M., Regan, M. O., Pawłowska, J., Rachold, V., Vonk, J. E., Werner, K., Wegner, C., Bennett, K. E., Vernal, A. D., Forwick, M., Fritz, M., Heikkilä, M., Łącka, M., Lantuit, H., Laska, M., Moskalik, M., Regan, M. O., Pawłowska, J., Promińska, A., Rachold, V., Vonk, J. E., Wegner, C., Bennett, K. E., Vernal, A. D., Forwick, M., Fritz, M., Heikkila, M., Lantuit, H., Laska, M., Moskalik, M., and Regan, M. O.: Variability in transport of terrigenous material on the shelves and the deep Arctic Ocean during the Holocene, Polar Research, 8369, https://doi.org/10.3402/polar.v34.24964, 2015.